THE RELATIONSHIPS BETWEEN DROUGHT SEVERITY, PRECIPITATION AND AEROSOL IN CALIFRONIA DURING THE 2012-2014 DROUGHT

A THESIS SUBMITTED TO THE GRADUATE DIVISION OF THE UNIVERSITY OF HAWAIʻI AT MĀNOA IN PARTIAL FULFILLMENT OF THE REQUIREMENTS FOR THE DEGREE OF

MASTER OF SCIENCE
IN
ATMOSPHERIC SCIENCES

May 2018

by
Jessica Marjorie Gartzke

THESIS COMMITEE
Committee Members:
Chairperson Jennifer Griswold
Pao Shin Chu
Alison D. Nugent

TABLE OF CONTENTS

ACKNOWLEDGMENTS

I would like to thank the University of Hawai'i Mānoa for provided me the setting to complete this work. The environment has been beautiful and supportive in every way. I would also like to extend my thanks to all the members of the Atmospheric Science Department, especially the professors who provided me with a quality education. Specifically, I would also like to thank my committee members, Alison Nugent and Pao Shin Chu for their helpful comments and constructive criticism, which challenged me to further improve my research. My deepest thanks goes to my academic advisor, Dr. Jennifer Griswold. She has guided me with patience and kindness that I never expected. I would also like to thank my undergraduate advisor, Dr. Robert Knuteson, for exposing me to research early in my academic career. Finally, I'd like to thank Nate Maier, Suzanne, Noelle and Charles Gartzke. With their loving support, I was able to thoroughly enjoy my graduate degree experience in Hawaii.

LIST OF TABLES

LIST OF FIGURES

Figure 13. MODIS aerosol time series beginning in 2002 and ending in 2016. The red solid line is the zero line. The black dashed lines demonstrate the first, second and third standard deviations of MODIS AOD. The top panel is averaged over the Northern half of California and the bottom panel is averaged over the Southern half.

Figure 14. P-values from the computed Wilcoxon Rank-Sum Test between (a) GPCP Precipitation and (b) TRMM precipitation (b) for Periods 1 and 5. The dots show the significantly different locations.

Figure 15. The significant locations (black dots) from the computed Wilcoxon Rank-Sum Test between MODIS AOD during the lowest levels of PDSI for the five months of the drought and MODIS AOD during the highest levels of PDSI for five month periods between 2002 and 2016. The difference between the two time periods is color shaded with greater values in yellow, oranges and red and negative values in green, cyan and blue.

Figure A1. Images showing the grid boxes that encompass the Northern and Southern regions of California. Green represents the area that was spatially averaged for Test 2 and Test 3.

Figure A2. Histograms of AOD and CER for DJF 2010 and JJA 2014 averaged for the entire state of California.

Figure A3. Histograms of AOD and CER for DJF 2010 and JJA 2014 averaged for the Northern half California.

Figure A4. Histograms of AOD and CER for DJF 2010 and JJA 2014 averaged for the Southern half California.

ABSTRACT

The 2012-2014 severe drought in California was notably destructive due to especially high temperatures and precipitation amounts lower than climatological means. This drought caused calamitous and far-reaching effects for the environment, economy and public health. Unlike previous periods of drought, understanding the causes of the most recent drought can now be accomplished through satellite-based measurements. Satellites offer global measurements of precipitation, temperature and aerosol; all of which can be used to estimate drought severity and impact. This study offers a 14-year climatology of precipitation, the Palmer Drought Severity Index (PDSI) and aerosol optical depth. The National Center for Environmental Information (NCEI) computes the monthly averaged PDSI for the state of California. Using this climatology of drought severity and MODIS Level 3 aerosol optical depth we can evaluate the impact drought intensity has on atmospheric aerosol loading. Increased aerosol has significant regional impacts including effects that directly impact communities, such as air quality and visibility, and impacts on the regional hydrological cycle by impacting cloud microphysical characteristics and precipitation. Precipitation observations from TRMM and GPCP are also analyzed in relation to PDSI. The amount of precipitation, its intensity, and duration are all important for determining drought severity and are considered here. The findings suggest a strong correlation between drought and aerosol, meaning that periods in severe drought tend to also correspond to high levels of aerosol loading in the atmosphere. We will also demonstrate precipitation and drought trends over the last 14 years.

CHAPTER 1: INTRODUCTION

1.1 Background

Aerosols are tiny particles suspended within Earth's atmosphere that can significantly affect regional and global weather and climate. These small particles can be emitted to the atmosphere in numerous ways, including anthropogenic sources and natural sources, both of which can be considered primary (emitted directly to the environment) or secondary (the result of interactions between primary pollutants, solar radiation, or other atmospheric constituents). Some of these sources include sea salt from oceans, mineral dust from arid locations, sulfate and nitrate from natural and anthropogenic sources and finally organic and carbon aerosols from biomass burning and industrial combustion. Improvements in remote sensing beginning in the early 2000's allow for better understanding of the Earth's atmosphere by providing global gridded data sets for a number of climate related components like aerosols. Using these tools scientists have been able to study many aspects of aerosol forcing, including global radiative forcing of aerosol. In addition, aerosols can serve as cloud condensation nuclei (CCN) impacting cloud properties and formation by changing cloud droplet size and concentration (Rosenfeld et al. 2008). This ultimately leads to changes in cloud properties, convection and precipitation (Koren et al. 2005). There is a positive correlation between aerosol and cloud microphysical dynamics suggesting aerosol is vital to understanding the earth system (Koren et al. 2010). Satellites have given scientists a new tool for investigating the magnitude of aerosol effects on weather and climate.

1.2 Cloud-Aerosol Interactions

Understanding the changes in cloud properties by the direct and indirect effects of aerosols is important for evaluating and predicting changes in weather and climate. It is known that cloud

droplets must form on preexisting particles suspended in the atmosphere or lofted from the surface. There are a multitude of aerosol processes that lead to changes in clouds and climate, both direct and indirect (Ramanathan et al. 2013). The direct effects of aerosol in the atmosphere relate to the influence of the aerosols on the planet's radiative balance by the scattering of solar and terrestrial radiation, and absorption effects that relate to Earth's radiative balance. These effects are not a concern for this work and will therefore not be discussed in further detail here. The indirect effects of aerosols on climate are the mechanisms by which aerosols modify the microphysical properties, amount, location and lifetime of clouds. The two main cloud changing mechanisms include the cloud albedo effect and the cloud lifetime effect (Lohmann 2006). Key parameters for determining indirect effects is the effectiveness of an aerosol particle to act as a cloud condensation nucleus, which is a function of the size, chemical composition, mixing state and ambient environment.

1.2.1 Indirect Effects

Increasing aerosol can change the characteristics of clouds, influencing cloud formation, development and precipitation processes. There are two main mechanisms by which aerosol affect precipitation (Sorooshian et al. 2009). The cloud albedo, or Twomey Effect, begins with an increase in aerosol that results in a larger quantity of cloud drops that are smaller in size as long as liquid water content is kept constant (Twomey 1974). Consequently, these smaller drops are slower to coalesce into raindrops. This works to suppress precipitation in shallow clouds and clouds with low liquid water content, effectively increasing the albedo of the cloud (Li et al. 2011). The cloud lifetime effect, or Albrecht effect takes the cloud albedo effect one step further. The cloud lifetime effect states that increased aerosol primarily suppresses precipitation resulting in clouds with more liquid water, higher fractional cloudiness and longer lifetimes (Albrecht

1989). Clouds, cloud systems and precipitation are, by nature, dynamically variable across space and time and the existence of many interacting feedbacks makes it difficult to directly attribute precipitation changes to aerosol perturbations (Sorooshian et al. 2009).

The following relationships exist when increases in aerosol concentration occur: (1) cloud droplets are smaller in size, (2) the lifetime of the cloud becomes longer, and (3) the cloud albedo increases. The connection between aerosol and clouds is relatively clear however, the relationship of aerosol to precipitation is not well understood. The number and complexity of the steps in the relationship between aerosols and precipitation makes quantifying these indirect effects challenging. Considering that precipitation from clouds plays the largest role in many drought indices, increased aerosol may be of concern to regions susceptible to drought (Rosenfeld et al. 2008).

1.2.2 Aerosol Studies in California

Studies on the effects of aerosol on precipitation in California have shown conflicting approaches. Some have shown that increases in anthropogenic sources of aerosol have reduced precipitation from orographic clouds because of the cloud lifetime effect (Lynn et al. 2007). In addition, increased aerosol has been shown to reduce snowfall rate due to the slowing of riming efficiency from orographic clouds (Lowenthal et al. 2011). Both of these effects pose a serious threat to California, where mountainous regions provide precipitation for much of the state water supply. Relatively clean oceanic air with low aerosol concentration flows from west to east over heavily populated and polluted locations before ascending over the Sierra Nevada mountain range downwind.

However, other studies contradict precipitation suppression by aerosol loading on the west coast (Ault et al. 2011). Besides local anthropogenic sources of air pollution, long range

transport of Asian dust via extratropical cyclones has been shown to enhance precipitation in California (Neiman et al. 2008). Through observational field studies like the CalWater and CALJET Campaigns, Asian dust aerosol has been linked to enhanced precipitation. This is based on observations that dust can effectively serve as ice nuclei, leading to increased riming rates and enhanced precipitation efficiency, which can contribute to enhancement in precipitation (Ault et al. 2011). These two mechanisms likely have counteracting effects on the relationship between aerosol, clouds, and precipitation in California. Although much work has been done to understand this relationship, including field campaigns and observational studies, distinguishing between meteorological, microphysical and thermodynamical factors is difficult. Field campaigns, which provide valuable in situ data, are infrequent and sample only small areas for a short period of time. By considering data from remote sensors, data can be obtained over large areas for extended time periods.

1.3 Drought Definition

Because of drought's far-reaching impacts on society, economy and the environment, studying drought is of great importance. Unfortunately, understanding and predicting drought is challenging. Even defining when a drought begins is difficult due to the fact that drought varies on both a temporal and spatial scale, resulting in many ways to define drought periods (Palmer 1965). Additionally, the geophysical, hydrological, meteorological, geological, economic and political sciences all understand and define drought from different viewpoints making it challenging to develop a definition that suits all cases. This work studies drought and uses the Palmer Drought Severity Index (PDSI) since it is the most widely used index in the field of Atmospheric Science. Palmer (1965) defines drought as a "prolonged and abnormal moisture deficiency." Although this definition seems vague, the generalized version can help atmospheric

scientists study drought in an objective way by providing a rigid and mathematical framework. Drought severity is also challenging to define considering it is dependent on duration, intensity, geographic extent and human water supply needs. To make quantifying drought more complicated, drought impacts is also heightened when a society is ill-prepared and vulnerable by reducing self-resilience (Wilhite et al. 2014). In many locations, the lack of proper infrastructure and policy further complicates the societal impacts of drought (Wilhite et al. 2014).

1.4 Societal Effects of Drought

Due to the nature of droughts, they tend to produce highly complex and spatially variable effects for the societal, economic and environmental sectors. Drought often has wide reaching effects that can ripple from regional to national to global in scale. These impacts are mostly due to the fact that many industries rely on water and precipitation for their goods and services. Destruction from drought, including reduced water supply, failing agricultural yields and even job loss, from drought tends to be a product of societal vulnerability and the severity of the drought itself. Impacts of drought are classified as direct and indirect (Svoboda et al. 2007). The direct effects include increased wildfires and reduction of crop yields. The indirect effects come into play as a byproduct of the direct effects. These may include unemployment, rising prices of goods and tax increases.

1.5 Drought in California

Drought is primarily a regional phenomenon. Furthermore, all indicators of drought must be considered on a regional basis (Alley 1984). A good example of an especially severe drought with far reaching implications is the most recent California drought between 2012-2014. With California's growing population and corresponding increasing water needs, the influence of this drought is of much interest to the scientific community. A physical representation of California

can be seen in Figure 1, showing large areas of desert, agricultural land and forested regions. Scientists have found through paleoclimate reconstructions that the severity of the 2014 drought is especially severe compared to past records, due to both the low water year precipitation and record setting warm temperatures (Griffin and Anchukaitis 2014). In fact, central and Southern California have had the lowest precipitation totals in the entire National Center for Environmental Information (NCEI) climatic record, going back 123 years. During this period, these low precipitation levels coupled with warmer than normal temperatures were found to exacerbate the impacts of precipitation reduction (Weiss et al. 2009). Furthermore, extended periods of precipitation reduction affect surface and subsurface water supply, reduces streamflow, groundwater, reservoir and lake levels. Figure 2 displays the mean temperature trend for the state of California showing an increase of roughly two degrees Fahrenheit between 1895 and 2016 (NCEI 2011). It has been shown that increasing temperatures in the southwestern region worsens precipitation reduction (Weiss et al. 2009). These very warm and dry conditions have serious impacts on agriculture, infrastructure, water supply and economic activity.

.

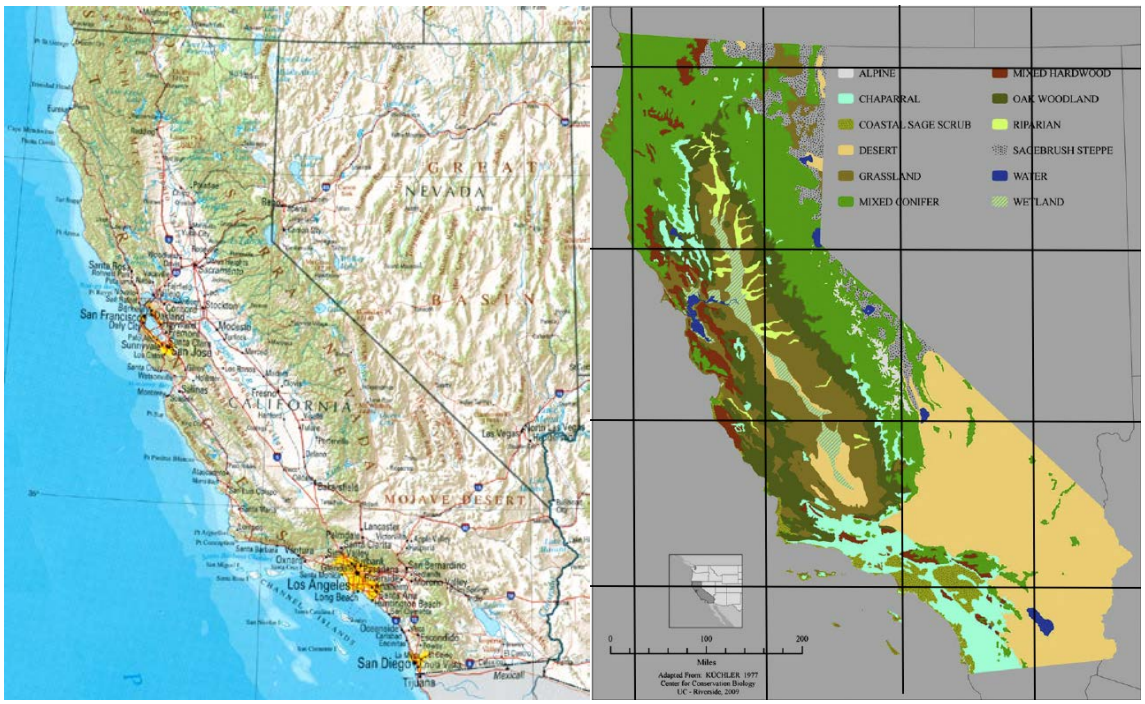

Figure 1. Physical (right) and vegetative (left) map of the state of California.

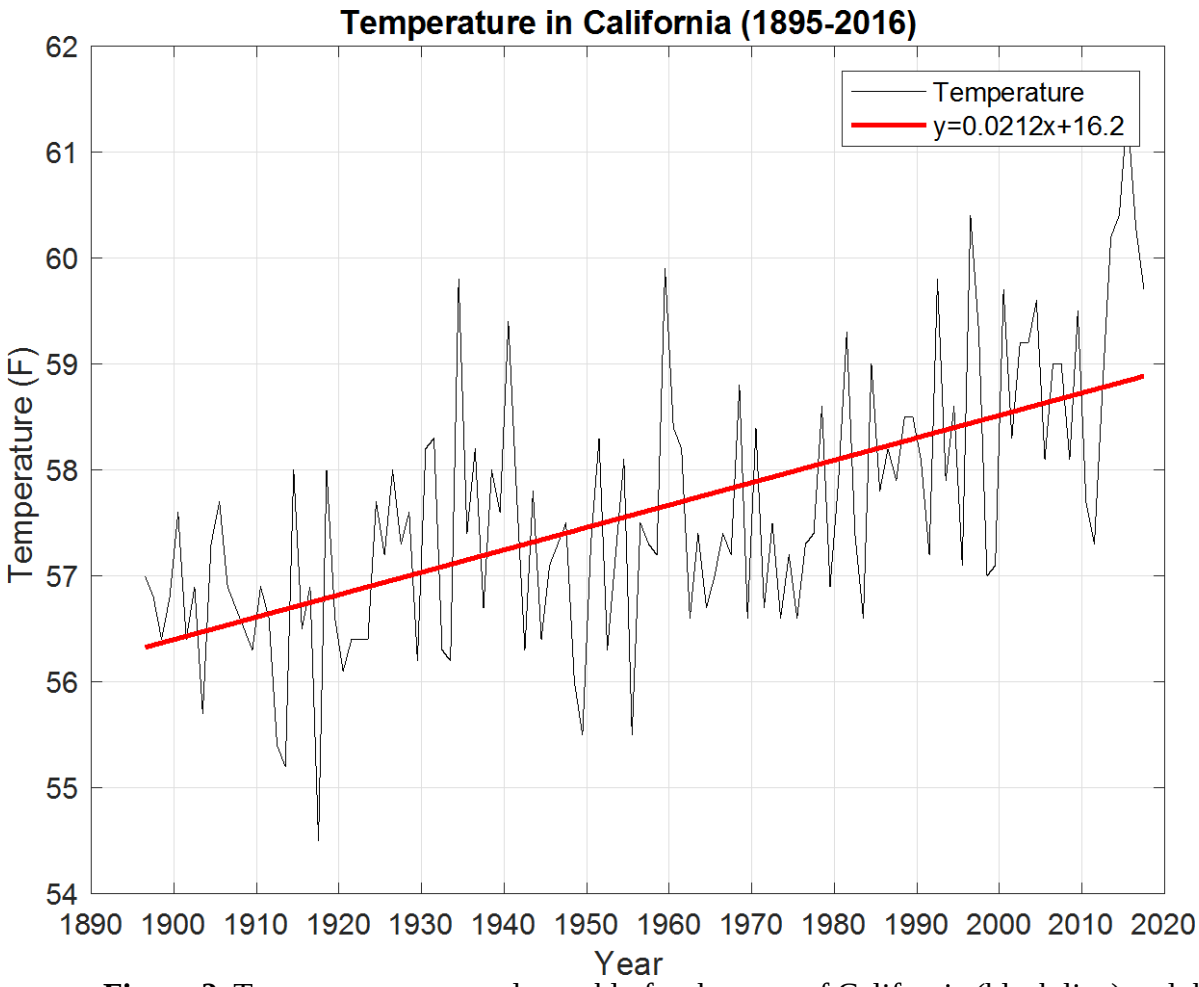

Figure 2. Temperature averaged monthly for the state of California (black line) and the 120-year trend (red line). The best-fit linear equation is given in the legend.

In addition, the population of California is a major concern for drought policy. According the United States Census Bureau, more people are moving to California more than ever before (U.S. Census 2016). California has seen a roughly 5.4 % increase in population since 2010, a factor greater than most other states and now has the largest population in the United States. The three year period from 2012 to 2014 was the most severe drought that California has experienced in the last 120 years (Griffin and Anchukaitis 2014). These findings tend to suggest there may be anthropogenic ties to drought severity. Furthermore, the number of drought occurrences in California has been greater in the past two decades than in the last century (Diffenbaugh et al. 2015). From climate models with and without anthropogenic influences it was found that human activities increase the likelihood that a dry precipitation year is also abnormally warm (Diffenbaugh et al. 2015). This human-influence will likely have wide reaching effects, especially is those areas of high population that demand strong agricultural production.

Agriculture is a large part of California's economy. The state of California is the largest contributor to economic and agricultural activity in the United States (Diffenbaugh et al. 2015), but unfortunately its biggest agricultural counties are in arid zones. Farmers have adapted to dry conditions and are now dependent on water harvesting and irrigation projects because the land is sensitive to rainfall and drought conditions. Some of these methods can cause further strain on the local water supply like groundwater pumping. The drought year 2014 cost California $2.2 billion in damages and 17,000 agricultural jobs (Howitt et al. 2014). Livestock was also affected due to the loss of usable pasture land. Almost $100 million in losses can be attributed to pasture loss from drought conditions in 2014 (Howitt et al. 2014). All in all, the 2014 drought is responsible for the greatest absolute reduction to water availability for agriculture ever seen in California (Howitt et al. 2014). This is largely due to the high agricultural demands and low

streamflow and reservoir levels. The seasonal cycle of drought in California is depicted in Figure 3 showing that the lowest and most severe months for drought tend to be in the summer growing season (June July and August). In addition, drought is affecting California's energy supply from hydroelectric power. Water reservoirs that also serve turbines supplying power are abnormally low. Reduced snowpack, reservoir levels and streamflow result in diminished surface water supply, which is worsened with increasing demand from the rapidly growing population in California.

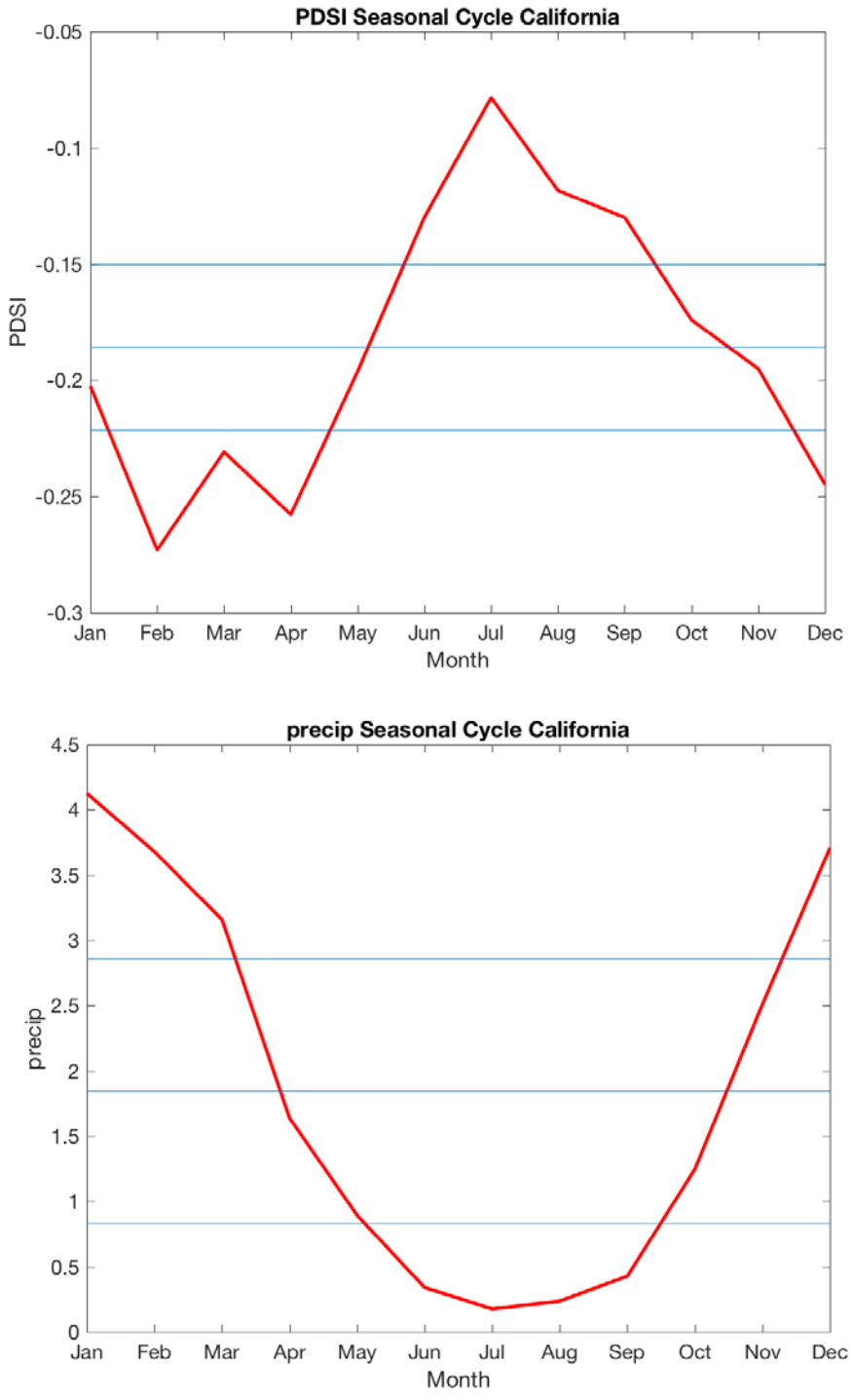

Figure 3. The seasonal cycle of PDSI (above) averaged from 1896 to 2016 over the entire state of California and the annual precipitation cycle (below) for California. The blue line is the mean for each data type.

Recent wildfires have worsened this phenomenon by limiting natural environments through fires. Drought allows for the extension of the wildfire season further into the fall and winter seasons leading to more wildfires with each year (Weiss et al. 2009). In addition, drought adds a component to intensify wildfires. Dry, hot and windy conditions along with dry vegetation tend to spark wildfires and increase their intensity and duration (Westerling and Swetnam 2003). These unpredicted changes to the natural environment of California will likely continue to affect the wildlife, wildfires and vegetation.

Increased rainfall may not alleviate symptoms of drought. Land-falling winter storms have large meteorological impacts on California by way of the precipitation from these systems (Ault et al. 2011). However, many factors affect the quantity of precipitation required to end or ameliorate a drought. Too much precipitation, like flooding, landslides and heavy snow, in a short timespan may not help alleviate a drought. Multiple winter storms must persist for an entire season before PDSI values begin to increase. Negative PDSI values are associated with drought and positive PDSI are non-drought or wetter periods. Once surface water recuperates, it may take years to fully recover from the depletion of ground water. The typical conditions that a region experiences during each month and season of the year is also essential (Karl et al. 1987). Given a drought of equal magnitude in a dry and wet climate, the wetter region requires more precipitation to end the drought by definition of PDSI. Thirdly, the season in which precipitation falls can also influence the amount of precipitation needed to end drought (Karl et al. 1987). All of these factors contribute to substantial challenges for water resource management, particularly maintaining the balance between water supply and flood mitigation.

1.6 Connections to a Positive Feedback Loop

In order to make connections within this study, a positive feedback loop provides a way to visualize the way drought, aerosol, cloud and precipitation relate. First consider some mechanism increases aerosol amount and that modifies cloud microphysical properties in the ways stated in Chapter 1.2.1. Smaller drops that coalesce into rain less effectively lead to local precipitation suppression. Precipitation suppression, if occurring during drought conditions, may exacerbate drought due to lack of moisture. Drought affects the amount of moisture in the top layer of soil by drying it to the point where individual dust particles can be easily lofted. These dust particles would then increase the amount of local aerosol thus completing a positive feedback loop. This work will concentrate on just one of the steps in this loop, mainly determining if aerosol increases during drought.

1.7 Study Objectives

The 2012-2014 Californian drought has been one of the worst in observational history as shown in Figure 4. This drought has affected more people and cost more money than any previously documented drought in Californian history. Remote sensing provides invaluable tools for understanding the mechanisms that cause drought. Using these advances along with surface based measurements can provide information about why droughts happen and how drought behaves. The first objective of this thesis is to make a quantitative assessments of the relationship between aerosol and drought in California. The second objective is to investigate this relationship of aerosol during drought and non-drought periods in California. The third objective is to understand how precipitation in California relates to aerosol.

1.8 Organization of Thesis

This thesis is organized as follows: Chapter 2 describes the data used for this work. Chapter 3 outlines the Methodology. Chapter 4 states the Results, Chapter 5 provides discussion and conclusions and Chapter 6 provides the references and acknowledgements.

CHAPTER 2: DATA

Aerosol, precipitation and PDSI make up the foundation of the analysis. Unfortunately, no instrument exists to measure all three variables in the same spatial, temporal and measurement methods. In order to produce the best results, data sources from both satellite and ground based sensors were used. The MODerate resolution Imaging Sounder (MODIS) was used for the analysis of aerosol (Remer et al. 2005). The Tropical Rainfall Measuring Mission (TRMM) and the Global Precipitation Climatology Project (GPCP) were used in conjunction to get the best estimate of precipitation (Adler et al. 2003; Kummerow and Barnes 1998). The NCEI's historical temperature and precipitation and PDSI record were used. A summary of each of these data sources is included here as well as a summary of how the PDSI is calculated.

2.1 The Palmer Drought Severity Index

Drought can be evaluated as a meteorological quantity and characterized by anomalous periods of severe precipitation deficit by the use of a drought index. In fact, attempts to quantify drought often make generic assumptions and over simplify many computations. Because of these simplifications, criticism of these indices is common because of the confusion different indices can cause for decision makers. Some even oppose the development of a drought index because a single number cannot properly take into account all of the needed environmental factors. Typically, drought severity is a function of drought magnitude as well as the duration of moisture deficiency (Palmer 1965). PDSI is one such index that considers variables such as temperature, precipitation, latitude of the location of interest, and the available water capacity of the soil (field capacity) and computes an estimate of drought severity. Some limitations of PDSI have been identified by Alley (1984).

There are two main issues to consider with the PDSI when calculating drought from a meteorological viewpoint. The PDSI algorithm region of interest has no political, geographical or vegetative boundaries which leaves this open to interpretation by the researcher. In addition, the highly criticized method for quantifying evapotranspiration from Dr, C. W. Thornthwaite was used in the calculation discussed in the next section (Palmer 1965; Thornthwaite 1948) . These limitations of the PDSI are valid, however, the PDSI is still the most widely used meteorological index for drought in the United Stated (Heim 2003) and provides good comparisons to larger grid boxes from remote sensors in space.

2.2 Palmer Drought Severity Index Algorithm

The PDSI calculation from Palmer is elaborate, as it incorporates many input variables and calculations. The first step in estimating drought severity is the moisture balance calculation (Palmer 1965). A two-layer soil concept is used to determine where in the ground layers moisture can be removed or added. The upper layer, or plow layer, is generalized to assume a holding capacity of one inch (25 mm) of available moisture. Therefore, it is assumed that evapotranspiration takes place in this layer until all the moisture is removed and at that time moisture from the second layer can then start in the process. Potential Evapotranspiration (PE) is then calculated using Thornthwaite's method (Palmer 1965; Thornthwaite 1948). Thornwaite's formula is essentially a measurement of potential evapotranspiration representative of the climatic demand for moisture (Palmer 1965). Other aspects of soil moisture balance like potential recharge (PR), potential loss (PL) and potential runoff (PRO) values are estimated. Palmer denotes these quantities as Climatologically Appropriate for Existing Conditions, meaning that information is transferred into coefficients that depend on the region being analyzed (Palmer 1965). The coefficients are as follows:

$$\alpha_{j=}\overline{ET_J}/\overline{PE_J} \quad (1)$$

$$\beta_j = \overline{R_J}/\overline{PR_J} \quad (2)$$

$$\gamma_j = \overline{RO_J}/\overline{PRO_J} \quad (3)$$

$$\delta_j = \overline{L_J}/\overline{PL_J} \quad (4)$$

where j represents months of year, *ET* is evapotranspiration, *R* is recharge, *L* is soil moisture loss, α is the coefficient of evapotranspiration, β is the coefficient of moisture recharge, γ is the coefficient of runoff and δ is the coefficient of moisture loss. The over bar represents the average of that quantity for a given monthly time period.

The second step is to subtract the actual precipitation from the average precipitation using the moisture balance coefficients. Note that for equation 1, $\alpha_j PE = (\overline{E_J}/\overline{PE_J)PE}$ therefore;

$$d = P_j - (\alpha_j PE_j + \beta_j PR_j + \gamma_j PRO_j - \delta_j PL_j) \quad (5)$$

where P is the areal average precipitation for a particular month.

The right side of the equation 5 is a simple water balance model. The total equation represents the departure from normal. It is defined as evapotranspiration plus runoff plus ground water recharge minus change in moisture storage. A weighting factor is then used to calculate the "moisture anomaly index" so that it can be compared to a variety of locations for any given month using the parameter "*K*" (Palmer 1965). *K* is determined from climate records using the following equations.

$$Z = K_j d \quad (6)$$

$$\text{where } K_j \text{ is a weighting factor } K = \frac{17.67\widehat{K_J}}{\sum_{j=1}^{12} D_i \times \widehat{K_J}} \quad (7)$$

$$\widehat{K_J} = 1.5 \ log_{10}(T_j + 2.8/D_j) + 0.50 \quad (8)$$

$$T_j = (\overline{PE_J} + \overline{R_J} + RO_j)/(\overline{P_j} + \overline{L_j}) \quad (9)$$

where T_j is a comparison between moisture demand and moisture supply. D is the mean absolute values of the monthly moisture departure. This moisture anomaly index (Z) varies between +/- 4.

After establishing a value for K_j then the values of Z are used to determine the monthly PDSI using the following equation.

$$PDSI_j = PDSI_{j-1} + \frac{1}{3}Z_j - 0.103(PDSI_{j-1}) \quad (10)$$

showing that the initial month in a dry or wet period is simply $\mathrm{PDSI_j} = \frac{1}{3}\mathrm{Z_j}$

The third term on the right hand side of equation number 10 is included so that when Z=0, or there is an average month, the PDSI value also approaches zero (Palmer 1965). In order to make this index have concrete meaning, Palmer divided the moisture anomaly index into different "classes" (Alley 1984). The index ranges from +/- 6 in value denoting dry (-) or wet(+) periods. If PDSI ≤ -4 there is extreme drought in that region. For example, a PDSI ≤ -3 is considered severe drought, PDSI of ≤ -2 is a moderate drought and a PDSI of ≤-1 is a mild drought. Finally, Palmer (1965) requires a reanalysis of the series to determine beginning and endings of drought and to develop a formula for drought severity for the region of interest. Palmer created a value P_e which can be considered a percentage probability that drought has ended.

$$P_e = \frac{\sum_{j=0}^{j=j^*} U_{i-j}}{Z_e + \sum_{j=0}^{j=j^*} U_{i-j} - U_i} \times 100\% \quad (11)$$

where $Z_e = -2.691(PDSI_{i-1}) - 1.5$ in a drought

and $Z_e = -2.691(PDSI_{i-1}) + 1.5$ in a wet spell

where U is the amount of dryness/wetness effective in ending a drought/wet spell.

Z_e is essentially the number in a single month that is needed to bring PDSI to -0.5 or 0.5. *U* is equal to *Z*+0.5 in a drought or *Z*-0.5 in a wet spell. For example, when P_e is 100% the drought is over. However, the drought is officially over any time P_e is greater than 0% and then continues to stay above 0% for some amount of time until it reaches 100% (Palmer 1965).

Although PDSI has numerous variable inputs, precipitation is the only term of importance for this study because we can consistently and constantly measure it from remote sensors.

2.3 National Centers for Environmental Information: Climate at a Glance

Monthly precipitation and PDSI values from 1895 to 2016 were retrieved from the United States Climate Divisional Database, available through the National Oceanic and Atmospheric Administration (NOAA) through their Climate at a Glance initiative and available from http://www.ncdc.noaa.gov/cag/time-series/us. The National Centers for Environmental Information (NCEI) has been monitoring temperature and precipitation across 344 climate divisions in the United States since 1895 (Guttman and Quayle 1995). These divisions are created to align with county boundaries and as many as 10 can exist in any one state (NCEI 2011). Users can select the city, state, regional and national data for a number of temperature and precipitation variables like average temperature, min and max temperature and heating and cooling degree days. Other drought indices include Palmer Modified Drought Index (PMDI), Palmer Hydrological Drought Index (PHDI) and Palmer Z index. Drought, and other climate indices have been derived from these data. These data are meant to be used to study large scale climate features and anomalies within the United States. The two sets of data from the NCEI platform were used in this analysis are PDSI and precipitation. PDSI was computed by the NCEI using Palmer's original method. Figure 4 shows the long term trend of PDSI. The best fit line

(dashed) shows the 1985-2016 trend. The years 2012, 2013 and 2014 are highlighted, all of which are well below the trend line. Initial analysis shows the extreme nature of the 2012-2014 drought.

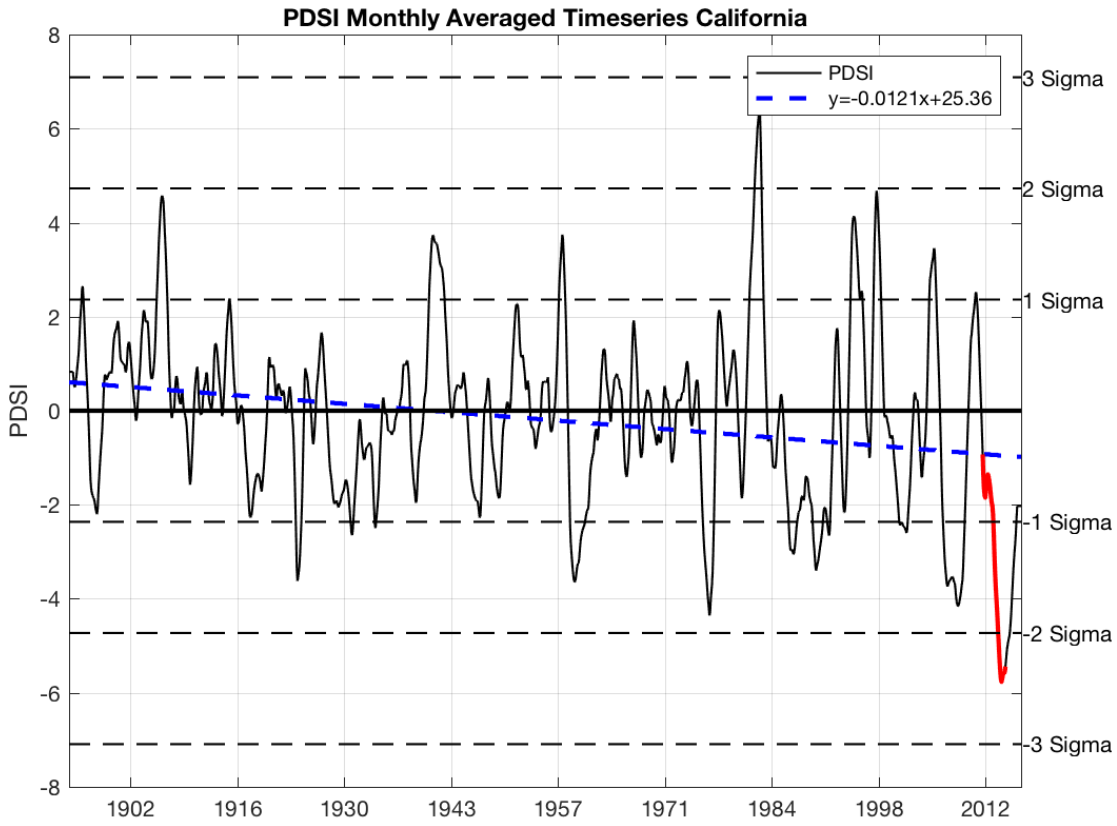

Figure 4. Time series of averaged monthly PDSI for the State of California from 1895 to 2016 (black) as well as a best fit linear line (blue dashed). The best fit linear equation is given in the top right. The 2012-2014 drought is highlighted in red.

2.4 MOderate Resolution Infrared Spectrodiometer (MODIS)

The satellite data used in this analysis was taken from the MODIS sensor on the Terra and Aqua satellites, which has been orbiting earth since 2002. Due to the nature of polar orbiting satellites, Terra MODIS and Aqua MODIS view the entire Earth's surface every 24 to 48 hours. MODIS acquires data in 36 spectral bands ranging from 15 to 41 μm (Remer et al. 2005). For example, MODIS is able to measure land, cloud and aerosol properties, ocean color, phytoplankton and biogeochemistry, atmospheric water vapor and temperature, atmospheric temperature, cirrus clouds, water vapor, cloud properties, ozone and surface/cloud temperature (Remer et al. 2005). This work will use solely, pixel-level retrievals, or MODIS Level 3 (L3). L3 data is an aggregation of Level 2 (L2) data onto a gridded 1 × 1 degree global grid to represent the statistics (mean, weighed means) of L2 products contained within grid square (Remer et al. 2008). These products are serviced by National Aeronautics and Space Administration (NASA) Goddard Earth Sciences (GES) Distributed Active Archive Center (DAAC) at http://daac.gsgc.nasa.gov/MODIS/.

The MODIS aerosol product retrieves ambient aerosol optical depth (AOD), particle size parmeters, mass concentration, asymmetry factor, backscattering ratio and the Ångstrom exponents over land and ocean globally (Kaufman et al. 1997). AOD is defined as the degree to which aerosols transmit solar energy by absorption or scattering and has no unit. It is essenitally the amount of aerosol in a column of air over a specific area. Measurments of cloud and aerosol using MODIS data have potential sampling and algorithm issues. This is due to the fact that MODIS does not have the ability to report cloud and aerosol in the same pixel. To prevent further error, the MODIS algorithm only uses pixels that have been recognized as having no cloud cover for reporting AOD. MODIS AOD can be used with a high degree of accuracy as

long as certain conditions are met. MODIS derived aerosol has been validated using the Aerosol Robotic Network (AERONET) measurements. In fact, MODIS has been shown to estimate AOD with an accuracy of 60% over water and 72% over land (Remer et al. 2008). Tanre et al. (1997) claims that MODIS derived AOD has an error of +/- 0.03 to 0.05 over oceans and +/- 0.05 to 0.15. All in all, MODIS allows for the better observations of aerosols because of its higher resolution than other existing sensors (Remer and Kaufman 2006).

Since aerosols are categorized by their size, often through a lognormal distribution, MODIS uses radius as a means of classification for their aerosol model (Remer et al. 2005). There are two MODIS algorithms, one for land and one for ocean. Depending on the algorithm there can be as much as 30% measurement error, this is partially due to optical geometry, clouds and nighttime measurements (Levy et al. 2009). Therefore, for comparison, this work uses MODIS Collection 6 (C6) Deep Blue AOD for best results.

2.4.1 Deep Blue Algorithm

The L3 Aerosol product from MODIS includes the Deep Blue algorithm which was developed to provide aerosol optical thickness over bright land areas like deserts, some of which have the greatest amounts of aerosol in the world (Levy et al. 2010). These data were retrieved from http://modis-atmos.gsfc.nasa.gov/. The algorithm consists of three separate aerosol optical depth retrievals: one for bright land, one for dark land and one for water. This addition to the original MODIS algorithm allows for improved sensing over deserts, which cover much of California. Compared to the previous version, MODIS Collection 5 (C5), C6 Deep Blue has improved cloud screening, a dust aerosol model and improved quality control screening (Hsu et al. 2015). The Deep Blue algorithm expands the coverage of aerosol products to include all snow free land surfaces including vegetated areas. C6 Deep Blue shows an improved correlation to

AERONET AOD measurements from 0.86 (C5) to 0.93 (C6) (Hsu et al. 2015). In addition, C6 data has nearly doubled the number of error free estimates, providing more global coverage.

Satellite retrievals of aerosol properties has proven to be invaluable for numerous fields of research, however, MODIS cannot see through cloudy regions. Therefore, spatial averages are utilized to get best estimates of aerosols. Although the retrievals will never be "true," a spatial average for a region can be used with confidence. Therefore, this study neglects the natural spatial variability of AOD at smaller scales than 1 × 1 degree, the resolution of MODIS AOD L3 data. Although a L3 global data was originally obtained, a subset for only the area encompassing the state of California was used for the years 2002-2016.

2.5 Global Precipitation Climatology Project (GPCP)

Reliable precipitation data has long been valued in the scientific community for uses in climate studies, societal applications, drought and industrial engineering. Therefore, quantifying precipitation is of vital importance, yet no single product provides the necessary coverage and accuracy to accomplish dependable precipitation estimates. The GPCP project is a combined data set that produces a global precipitation analysis. Combining data from many sources to form one large global compilation is complex because there is no single type of measurement that covers the entire globe with accuracy. Sources of precipitation data include rain gauge and soundings as well as low orbit and geosynchronous satellite observations. The data is formatted in a 2.5 × 2.5 latitude-longitude grid and covers the time period 1979 to 2016 (Huffman et al. 1997). The merging of microwave sensors, infrared sensors and gauge data were taken advantage of each data sets' strengths. For example, the remote sensing data has good temporal resolution but tends to preform best under deep convection situations (Huffman et al. 1997). In order to produce the global gridded dataset, a blending procedure was created for combining these data

sets based on Huffman et al. 1997. The initial results of Huffman et al. 1997 show fair agreement with existing climatology (Huffman et al. 1997). In addition, the global products include uncertainty due to a random error calculation for best analysis due to the high level of difficulty in the blending algorithm. The complex nature of adapting satellite data to grid based quantities can cause error. This analysis method changed from V1 to V2. Version 2.1 included an update of the gauge input dataset and Version 2.3 now includes data from the SSMIS satellite. The data for this study was retrieved from https://www.esrl.noaa.gov/psd/data/gridded/data.gpcp.html with the product name

precip.mon.mean.nc.

2.6 Tropical Rainfall Measuring Mission (TRMM)

Although precipitation is one of the key components of the hydrological cycle, high spatial resolution data has long been lacking in measurements of precipitation. Before satellite data, rain gauge and other point-measurements were used but provided limited spatial resolution. The TRMM mission was developed to address this issue and fill gaps in our knowledge of the hydrological cycle (Kummerow and Barnes 1998). The goal of the NASA and the National Space Development Agency was to measure rainfall and energy exchange in the tropics and the subtropics (Kummerow and Barnes 1998). The last two years (2015 and 2016) of data included in this analyses (Product 3B42) is a collection of multiple independent precipitation estimates from the TRMM Microwave Imager (TMI), Advanced Microwave Scanning Radiometer for Earth Observing Systems (AMSR-E), Special Sensor Microwave Imager (SSMI), Special Sensor Microwave Imager/Sounder (SSMIS), Advanced Microwave Sounding Unit (AMSU), Microwave Humidity Sounder (MHS), and microwave-adjusted merged geo-infrared (IR) (Huffman and Bolvin 2017). GPCP provides longer and more consistent record, from 1979 to

2016, for climatological comparisons. These instruments include a microwave imager (MI), precipitation radar (PR) and the Visible and Infrared Radiometer System (VIRS). The satellite also caries Earth Observing Systems including the Clouds and Earth's Radiant Energy System and the Lightning Imaging system. This combination of passive and active instruments provided three dimensional coverage of the global tropical regions (Kummerow and Barnes 1998). The data covers an area from 50° S to 50° N for all longitudes and the satellite orbited at 350 km with a 35 degree inclination angle (Kummerow and Barnes 1998). The data became available starting in 1997 and ended in 2015, with the combined data set (without TRMM) expected to continue to 2018 (Kummerow and Barnes 1998). Kummerow at al. (1998) summarizes the updates to the TRMM project after two years of use. The improvements of the project show an increase of 24% (Version 5) for global monthly averages and show promise for future studies. The data used for this study was retrieved from https://pmm.nasa.gov/data-access/downloads/trmm. TRMM 3B43 Version 7 retrievals between 1998 and 2016 were used at 0.25 by 0.25 ° resolution. The 3B43 dataset merges the daily 3B42 dataset with the GPCP rain gauge analysis because it can provide better large scale climate estimates when merged with remote sensing techniques. In order to get a visual representation of the three precipitation data types that were used in this study, Figure 5 shows the time-series NCEI precipitation (mm/day) between 1895 to 2016 overlaid with TRMM and GPCP precipitation data. It provides visual context and comparison between the three types of data. NCEI has the longest record followed by GPCP and TRMM but they all overlap in time so comparisons between them are possible. Notice the annual fluctuations patterns agree between the three data sets. The TRMM merged satellite analysis indicates fairly close agreement with the GPCP estimates however, notice the GPCP precipitation levels show significantly lower values of precipitation than NCEI and TRMM. The GPCP analysis is done at 2.5 × 2.5 degree

latitude/longitude resolution and has different retrieval methods and averaging algorithms than TRMM. The same features are evident but there are subtle differences in the magnitudes (Adler et al. 1999). TRMM based estimates have higher peaks that match up with NCEI peaks. Because GPCP emphasizes long term climate trends, data is averaged spatially over a much larger area than TRMM, many of the extremes in precipitation can be lost.

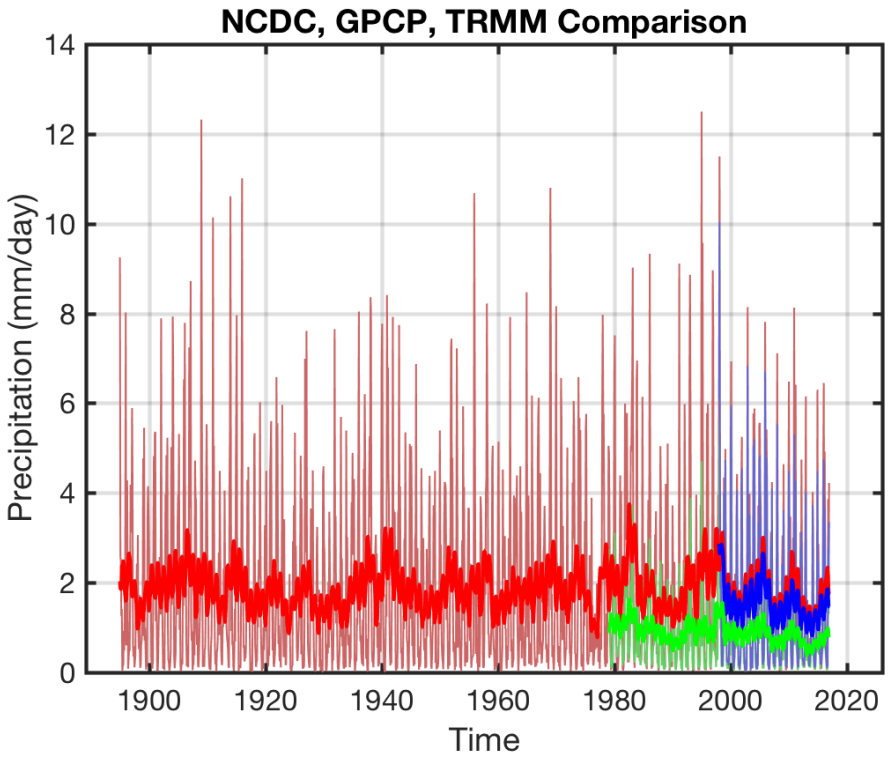

Figure 5. Time series for all precipitation data used in this analysis including 1) NCEI (red) going back to 1895, 2) GPCP (green) going back to 1979, and 3) TRMM (blue)starting in 1998.

Chapter 3: Methodology

3.1 Data Extraction and Processing

The entire record of precipitation and PDSI from NCEI, precipitation from the TRMM and GPCP projects and aerosol from MODIS were obtained. The NCEI data was collected in such a way that little data processing was needed to complete the 120-year time series. In contrast, the remote sensing data required detailed processing in order to be scientifically valuable to this project. For each month, a box roughly 12.5 × 12.5 degrees latitude and longitude was extracted around California for each of the following data sets: TRMM, GPCP and MODIS. Then, an ocean and land mask was created to fit and applied to the extracted data and applied. This allowed for a complete and accurate comparison of the data. The land-ocean mask only includes the land mass area of California but not the ocean for comparison with a collection of ground based measurements from NCEI. Figure 6 shows an example of GPCP data with and without the ocean mask.

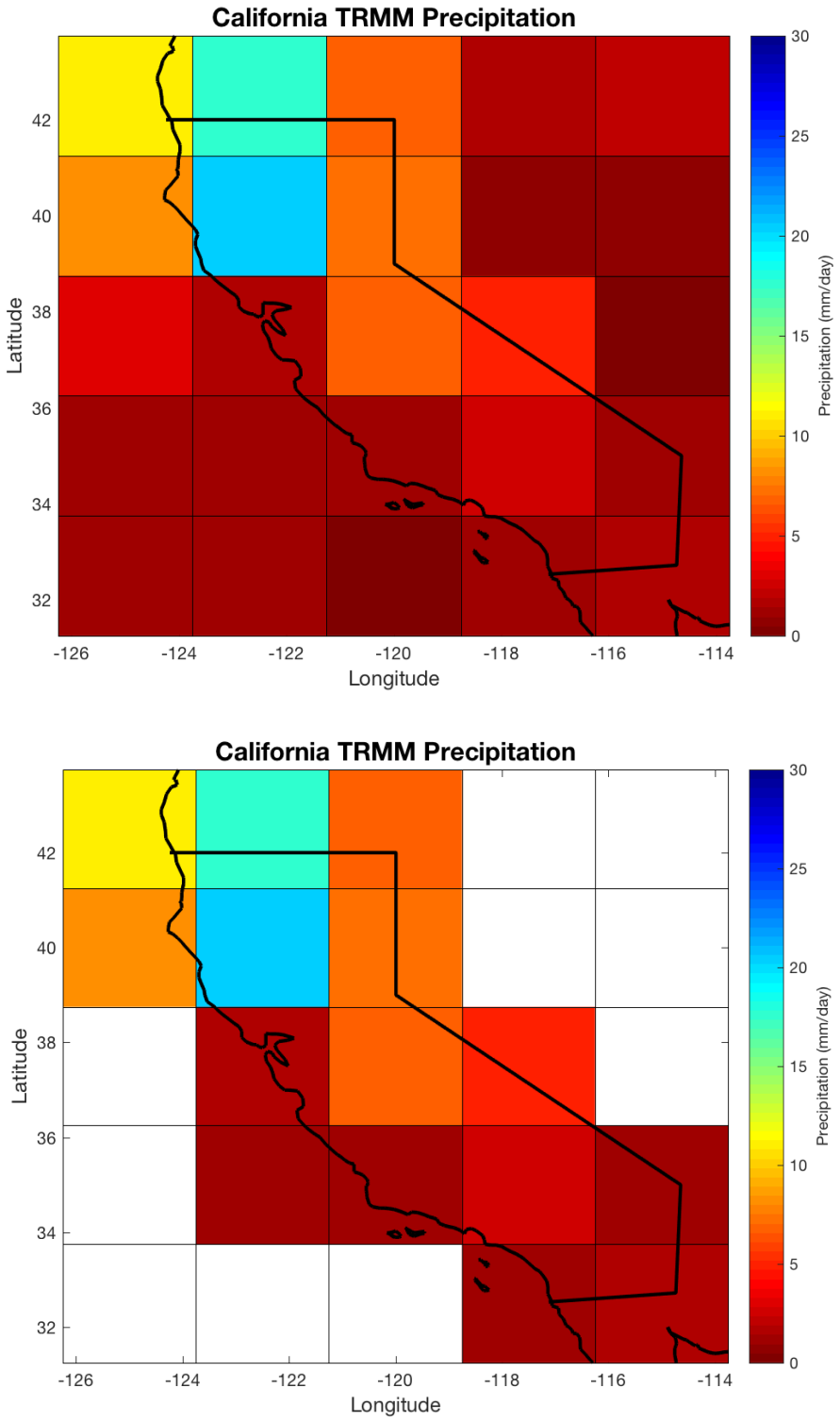

Figure 6. An example of the land ocean mask used for TRMM data for the state of California averaged for the month of January 1998. Without a mask (top) and with a mask (bottom).

3.2 Annual Cycle Selection Periods

Precipitation in California exhibits spatial, topographical and seasonal cycles. Subdividing the data into seasons helps to show clear distinctions between wet and dry periods as well as revealing their individual trends. Since precipitation patterns along the West Coast are strongly related to local and large scale circulation patterns and have high seasonality, there tends to be a distinct wet and dry season in California shown in Figure 3 (Cayan and Roads 1984). By looking at wet and dry periods individually, more in-depth analysis of drought periods can be achieved. The annual precipitation cycle is distinct with a maximum in the winter and a minimum in the summer (Cayan and Roads 1984). Winter brings frontal systems with rain and snow while the summer is characterized by hot and dry conditions(Weiss et al. 2009). In this work, the "wet" season is determined to be December, January and February (DJF) while the "dry" season is the months of June, July and August (JJA).

3.3 PDSI Selection Periods for Wilcoxon Mann Whitney Rank Sum Tests

The long term time-series PDSI values for California were examined using the NCEI climatological data. Using a 13-month running average, we computed trend lines for two time periods: 1895-2016 and 2002-2016. The 13-month average was chosen to avoid yearly average issues. From Figure 7, both lines show a substantial decrease over time meaning more severe drought is prevalent in recent years. In addition, the difference between the two rates of decrease is large. Between 1895 and 2016 there was a reduction of about 0.121 PDSI/decade while the 2000's show a more extreme decrease of 2.77 PDSI/10 years. It can be stated that between 2002 and 2016, drought in California has become more severe than ever in the 120-year climatology.

A focused analysis of this same trend reveals 5 local minima and maxima between 2002 and 2016 seen in Figure 7.

In order to compare the 2012-2014 drought to other non-drought periods, corresponding periods of positive PDSI, negative PDSI and neutral PDSI were chosen. Figure 7 demonstrates the PDSI trends between 2002 and 2016. The local minimum and maximums during the 14-year period were calculated. These represent the recent drought and non-drought periods in California. MODIS Aerosol data was extracted for the 2 months on either side of the local min or max, to identify a 5-month period of time, sufficient for the analysis. The five-month extraction period was chosen to get the best representation of the drought or non-drought aerosol characteristics during that time. By comparing these five 5-month time periods, conclusions can be drawn to reveal the relationship between PDSI and aerosol in drought and wet periods. Table 1 summarizes the 5 periods used for analysis. Each minimum and maximum is labeled period 1 through 5 consecutively.

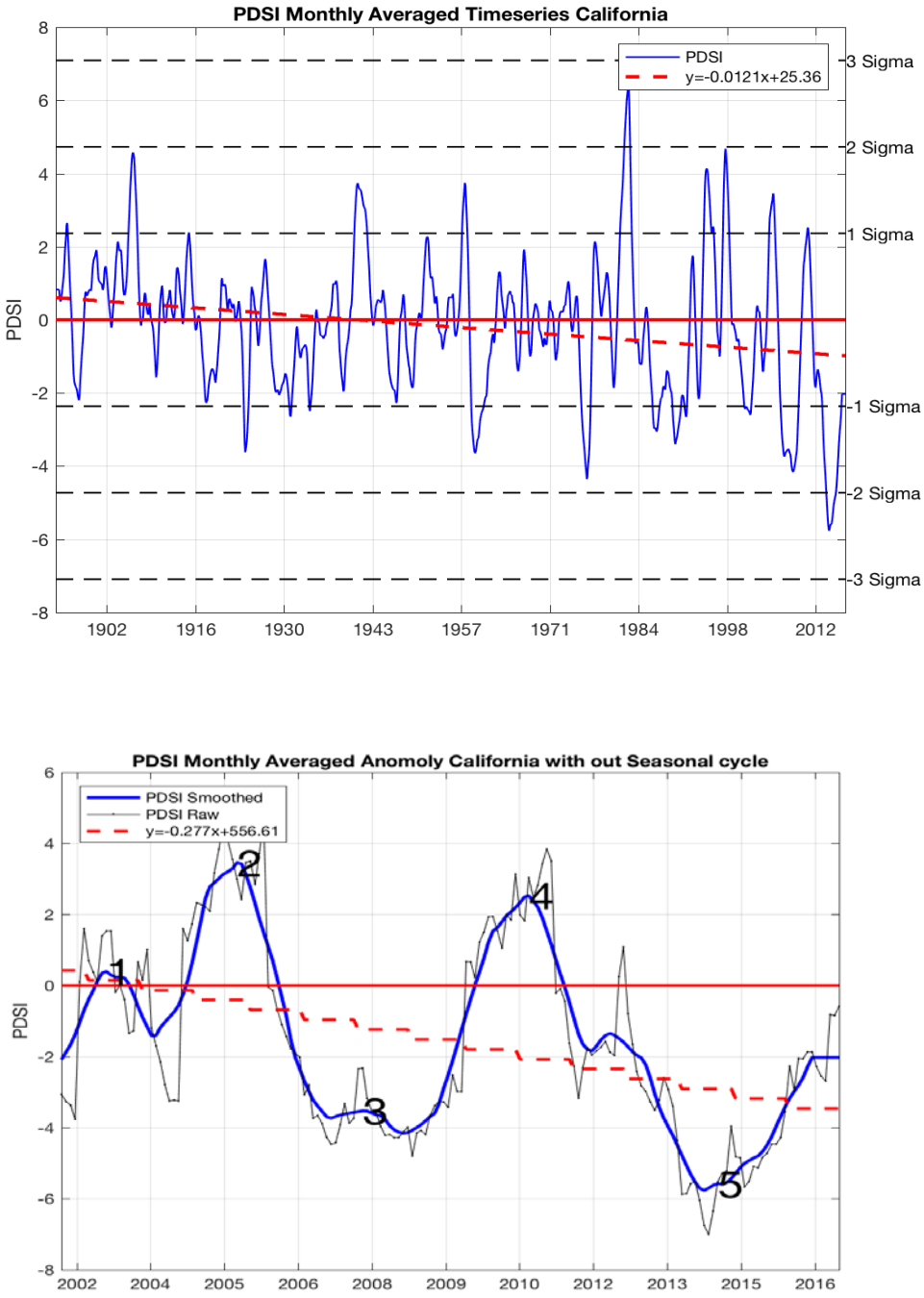

Figure 7. (Top) PDSI averaged monthly and fit to a 13 month running average (blue) for the State of California from 1895 to 2016 as well as a best-fit linear line (red dashed). (Bottom) PDSI for California from 2002 to 2016 with the 13-month running mean (blue) the raw data (black), and a linear fit (dashed red). The zero line is highlighted in solid red. Black numbers are displayed as the five local minimum and maximums between 2002 and 2016.

Period Number	Local Min/Max	Extracted 5-month period	PDSI Min/Max	PDSI Classification
1	May 2003	March 2003 – July 2003	0.5	Near Normal
2	October 2005	August 2005 - December 2005	4	Extremely Wet
3	February 2008	December 2007 – April 2008	-4	Severe Drought
4	March 2011	January 2011– May 2011	4	Extremely Wet
5	September 2014	July –2014 - November 2014	-6	Severe Drought

Table 1. Table summarizes the selected periods for data analysis extracted from Figure 7.

3.4 Data Re-gridding

TRMM data were re-gridded from 1 × 1 degree to match the GPCP grid resolution of 2.5° × 2.5° using a linear interpolation process in both the latitudinal and longitudinal directions. Both data sets were used because of TRMM's tendency to lose skill at higher latitudes, especially poleward of 40 degrees (Nesbitt and Anders 2009). Unfortunately, California is located at the top of TRMM's domain between 30 and 42 degrees north. In addition, the entire TRMM satellite was unavailable starting in April 2015. In addition, the comparison between two remote sensing packages like TRMM and GPCP provide confidence in the precipitation data used in this study. Figure 8 shows an example of TRMM that was re-gridded to match GPCP. Next, statistical analysis was done to the monthly averages of GPCP precipitation and TRMM precipitation data, to determine specific grid boxes in which the correlations with precipitation and aerosol were especially relevant.

Both GPCP and TRMM data were used for two reasons. First, they provide additional validity to the precipitation data included in this study. Second, TRMM and GPCP products, by nature of the products, have different benefits for this analysis. TRMM provides high resolution data useful for specific events or locations while GPCP provides a medley of data sources and better overall coverage. GPCP tends to be useful for climatological purposes.

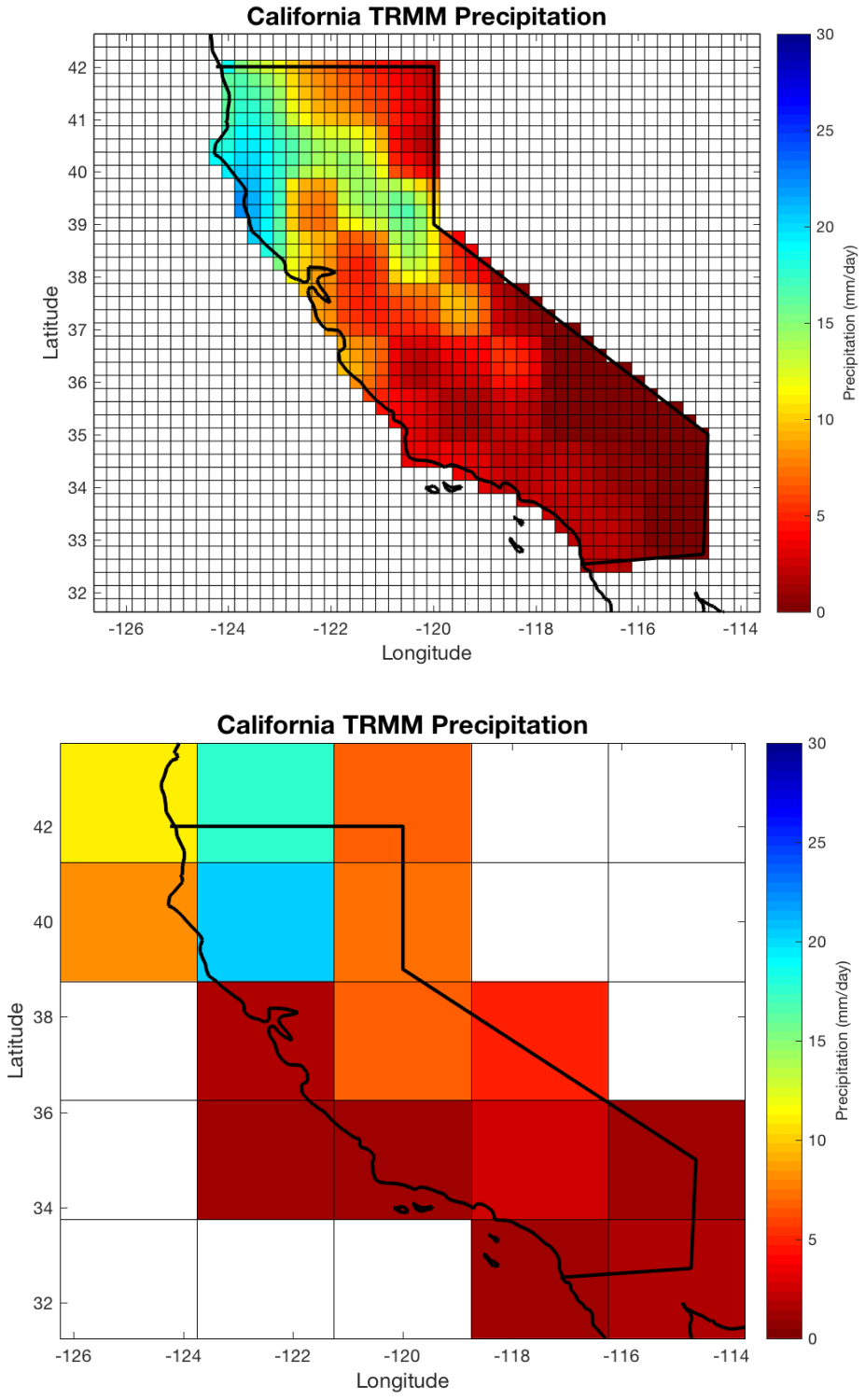

Figure 8. An example of TRMM precipitation re-gridding from 1x1 degree to 2.5 x 2.5 degrees over California view for June 2014.

3.5 Wilcoxon Mann Whitney Rank-sum Tests

To statistically analyze two independent data sets that are not necessarily normally distributed, the Wilcoxon Rank Sum Test was used (Wilcoxon 1945; Mann and R. 1947). This non-parametric test essentially evaluates whether a value (i.e. location) from one sample is greater or less than a value from the other sample (Chu and Chen 2005). This produces a yes or no that determines if the null hypothesis is accepted or rejected. The null hypothesis is that any difference between two samples is due to random chance. The Matlab function ranksum was used to calculate both a probability of occurrence (*p* value) for combinations of precipitation and aerosol, drought and aerosol and drought and precipitation. This function calculates a z-statistic below to approximate the *p*-value and then determine if the null hypothesis is rejected. Very low *p*-values indicate the rejection of the null hypothesis of equal medians at the 5% significance level (α=0.05).

$$z = \frac{R - \mu_g}{\sigma_g}$$

where

$$\mu_g = \frac{n_1(n_1 + n_2 + 1)}{2}$$

and

$$\sigma_g = \sqrt{\frac{n_1 n_2 (n_1 + n_2 + 1)}{12}}$$

R is the sum of ranks for the smaller sample size n_1. n_1 is the smaller of the sample sizes. n_2 is the larger of the sample sizes.

p-values were computed for each of the grid boxes encompassing California using a look up table and the method stated above. As stated earlier, TRMM data were re-gridded to fit GPCP for

better comparisons. Each grid box for the MODIS AOD extracted periods data was compared to the corresponding grid box for every combination of time periods 1 through 5. This produced maps showing the locations that have statistically significant aerosol between time periods.

CHAPTER 4: RESULTS

4.1 Aerosol, Precipitation and PDSI Relationships

First, Pearson correlations between the ground-based NCEI temperature, precipitation and PDSI data were computed as well as MODIS AOD, TRMM precipitation and GPCP precipitation in order to investigate their statistical relationships. Daily data from MODIS, TRMM and GPCP were converted to monthly averages to allow for a direct comparison to the lower temporal resolution NCEI data. The results are summarized in Table 2. The Spearman rank-sum correlation is simply the Pearson rank correlation coefficient between two ranked variables and measures the strength and direction of the association between them. In addition, AOD is correlated with NCEI precipitation (r=-0.652) and PDSI (r=-0.390). AOD and NCEI precipitation show a similar relationship to the remote sensors, GPCP and TRMM. This relationship is negative suggesting greater precipitation correlates to less aerosol amount. However, the AOD and PDSI analysis shows a poor negative correlation with scatter around -2 PDSI. Scatterplot analysis was also completed for other aerosol and precipitation relationships as seen in Figure 9 and 10.

Figure 9 shows the NCEI PDSI and precipitation anomaly scatterplot highlighting the 2012, 2013 and 2014 values. A best-fit line is used to mimic the trend of the data to provide information about the actual relationship. This line is not a threshold for drought, it just provides a linear regression. It is clear that most the 2012-2014 values are below the zero-line, demonstrating the severity of the drought. PDSI and precipitation show a slightly positive correlation meaning that with greater precipitation, greater values of PDSI are likely. Note that that any PDSI value less than zero are considered drought. Although not very strong, the PDSI-Precipitation correlation suggests that even greater levels of precipitation do not correlate exactly

to more positive PDSI (wetter). There is much variation in PDSI at periods which are close to zero. These data are considered "transition periods" meaning they are times when the PDSI is transitioning from negative to positive. These variable PDSI values show that even though precipitation is considered to be in a "moisture deficit", PDSI values are not always raised by a particular precipitation event or even several precipitation events. Thus varying amounts of precipitation and negative PDSI values are possible.

Figure 10 shows that both GPCP and TRMM precipitation with MODIS AOD show negative correlation coefficients of r = -0.690 and r = -0.657 respectively. This means that for greater AOD, less precipitation is likely. This trend of greater precipitation matched with decreased observed aerosol is expected because of precipitation scavenging. This process involves the removal of particulate matter from the atmosphere by hydrometers (Radke et al. 1980). As part of this process, the atmosphere is "cleansed" and balanced between the sources and sinks of aerosol.

	MODIS AOD	NCEI PDSI
GPCP precipitation	-0.690	X
TRMM precipitation	-0.657	X
NCEI precipitation	-0.652	0.317 Wet Season 0.637 Dry Season 0.190
NCEI PDSI	-0.390	X

Table 2. A compilation of spearman Rank coefficients for each combination of PDSI, AOD and precipitation data.

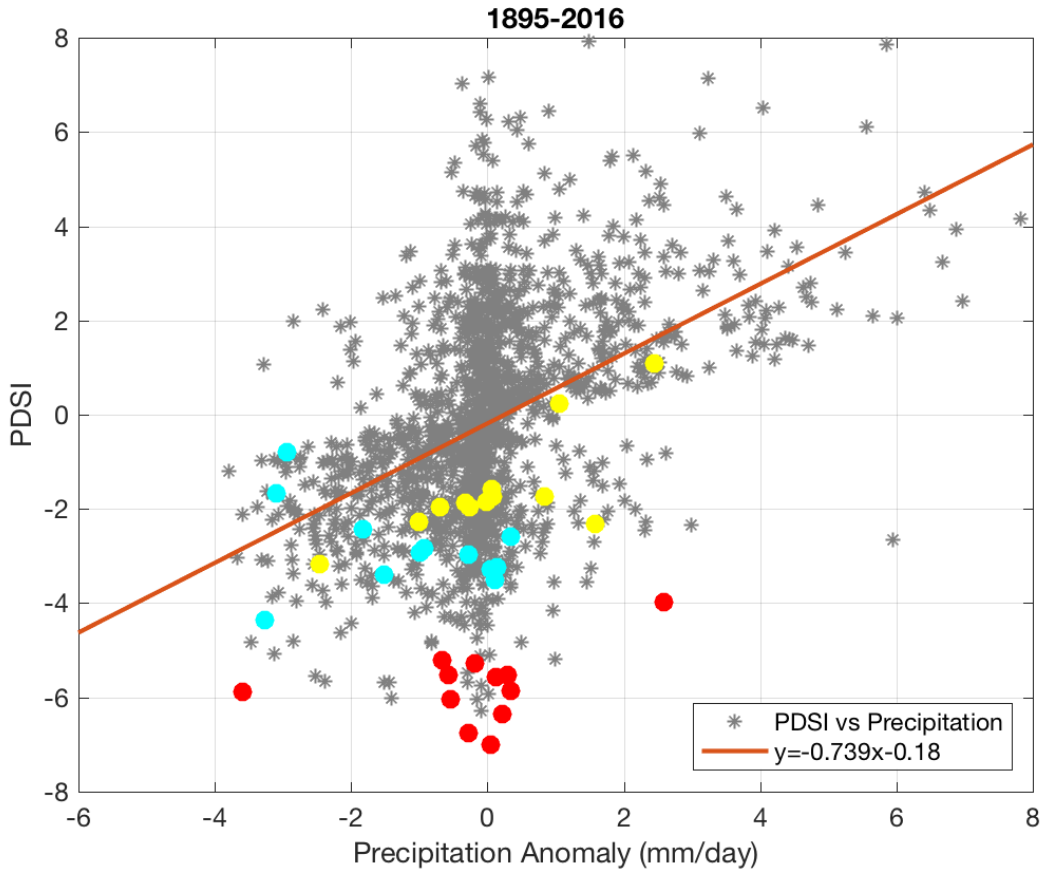

Figure 9. PDSI and precipitation anomaly data from NCEI matched for monthly means. 2012 values (yellow), 2013 (cyan) and 2014 (red) circles dots represent these years' values.
The best fit line is given in red and written in the bottom right hand corner.

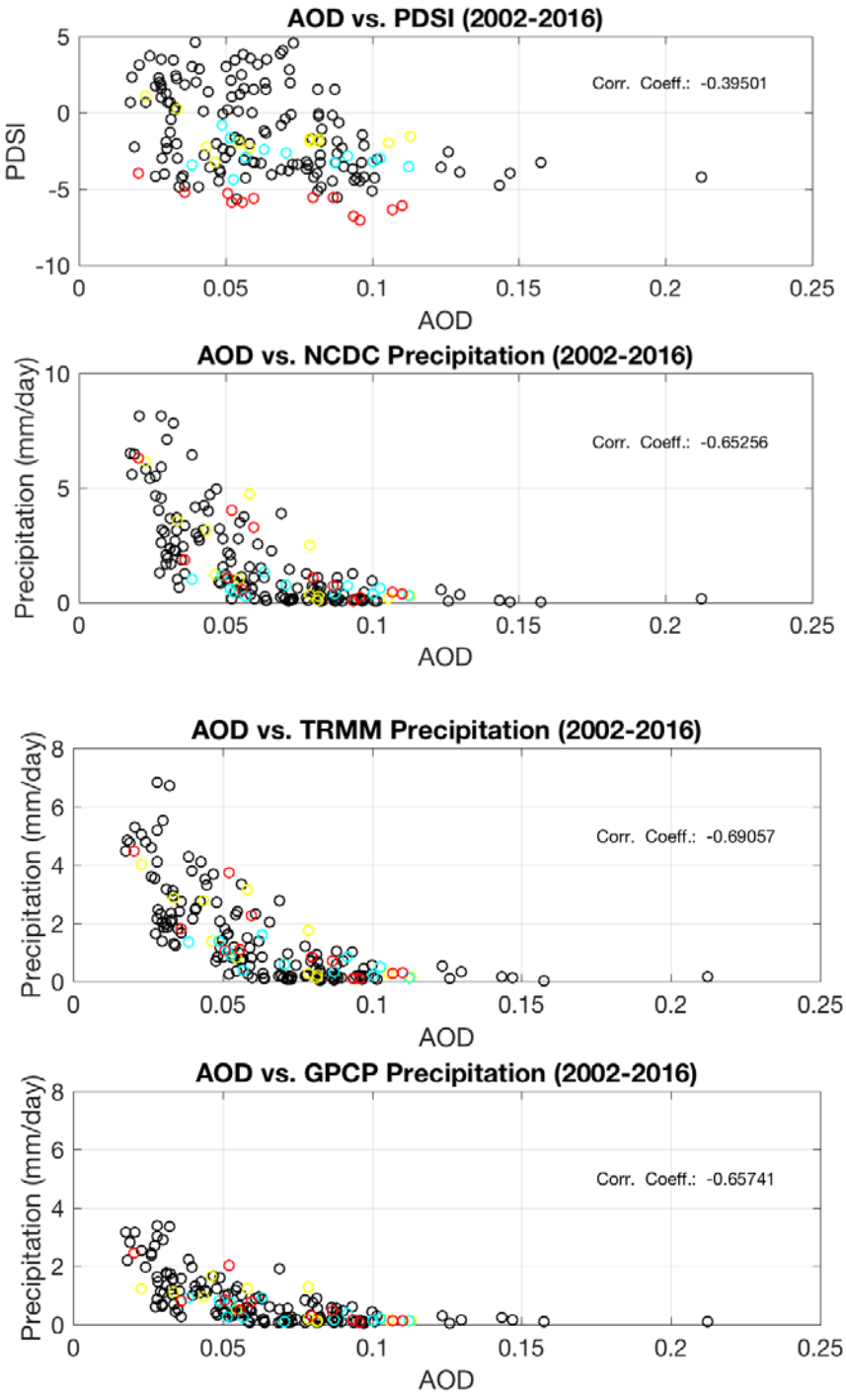

Figure 10. Scatterplot displaying the correlation between MODIS AOD and NCEI precipitation and PDSI (a + b) and MODIS AOD with TRMM and GPCP precipitation (c + d). 2012 values (yellow), 2013 (cyan) and 2014 (red) circles dots represent these years' values. You need to fix those text boxed, they looked weird and then I found all that random text hidden.

a.

4.2 Box plot Analysis

An analysis of the seasonal differences of PDSI and precipitation from NCEI surface observations from 1895 to 2016 was completed. Looking back to Figure 3, we see the seasonal rainfall cycle averaged for the state of California. Although precipitation does occur in the months of November, March, and April, the highest precipitation accumulations tend to be during the winter months of DJF. Box and whisker plots for both precipitation and PDSI data for each wet (DJF) and dry season (JJA) are shown in Figure 11. The boxplots represent the median, the 25^{th}, 50^{th} and 75^{th} percentile of the data as well as any outliers above 3/2 of the upper quartile and below the lower quartile.

As expected, mean precipitation in the dry season (0.251 mm) is much less than the wet season (3.84 mm) and varies less, suggesting different mechanisms work to enhance or suppress precipitation and these mechanisms vary throughout the year. These mainly include the albedo and lifetime effect as mentioned in Section 1.2.1. Yet in general, both wet and dry season precipitation is positively skewed, suggesting lighter precipitation over California is more likely than heavy precipitation. The width of the distribution for the wet month's precipitation is much broader than that of the dry month's suggesting greater variation in precipitation in the wet months. The wet and dry season PDSI boxplots show an evenly distributed sample. The wet season mean PDSI is slightly lower than that of the dry season even though the dry season has a greater standard deviation. This result warrants some possible explanations. Because of the way the index was designed, the PDSI algorithm does not depend on precipitation alone. The calculation involves many input variables and climatological indices that may affect the entire PDSI calculation, even when precipitation occurs. Furthermore, in a drought situation, even

though precipitation may be much greater in the wet months, the amount may not be enough to fully modify the state out of drought.

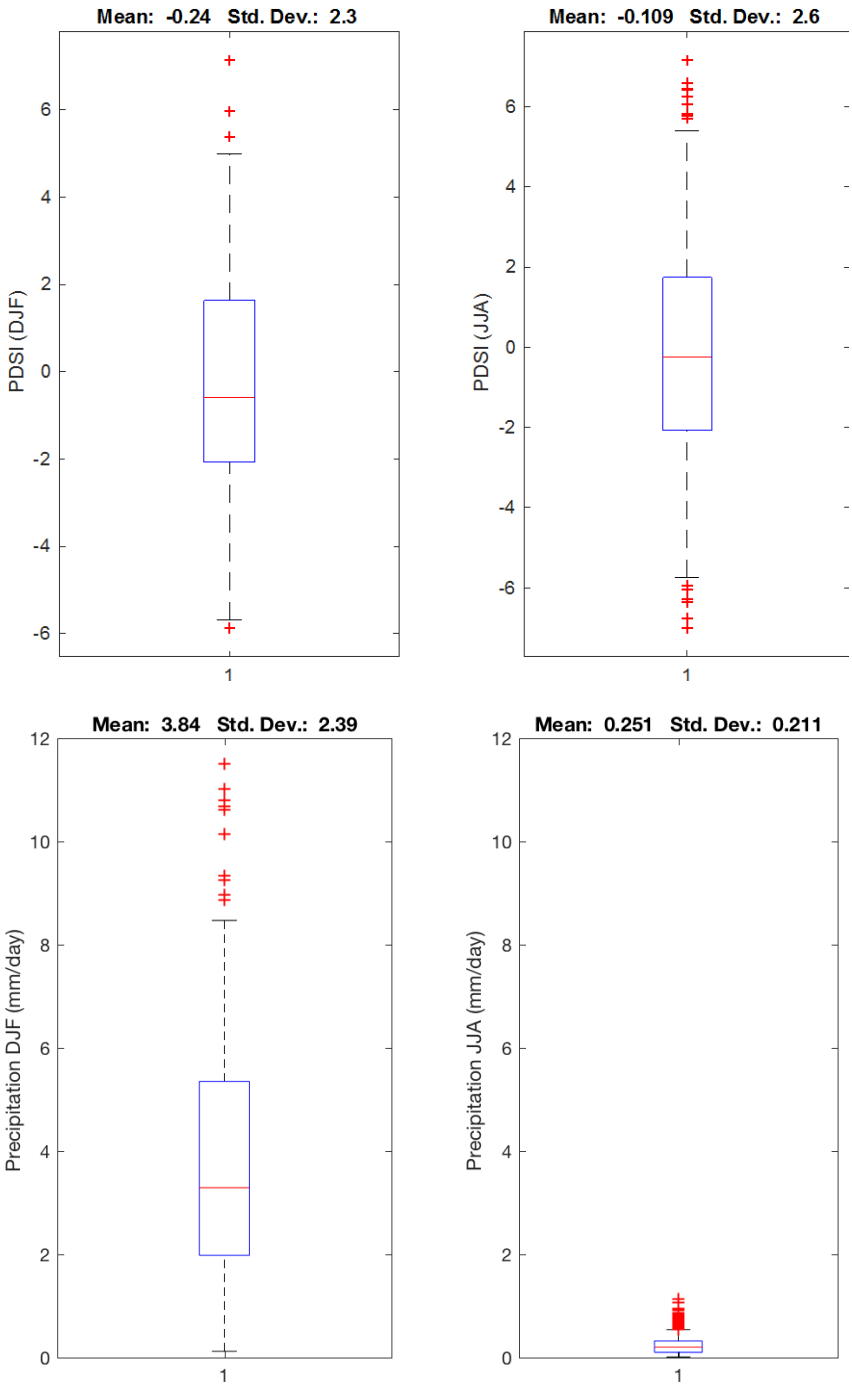

Figure 11. Box and whisker plots of NCEI data on the y-axis, with PDSI values (above) and precipitation in mm (below) on the left describes the wet season (DJF) and the right describes the dry season (JJA). The red lines represent the median point in the data. The red plus signs represent any outliers in the data that are more than 3/2 times the upper quartile.

4.3 Aerosol and PDSI Trends

Time series plots provide a descriptive analysis for the trend estimations, seasonal patterns, and predictions. However, the biggest advantage of time series analysis is that it can be used to understand the past as well as provide some estimation of future values. This feature of time series analysis is ideal for studying drought because of its strong ties to cyclical patterns.

The entire MODIS AOD record was used to create a 14-year time series of monthly averaged aerosol for the state of California. From Figure 12, AOD shows no distinct long-term trend, with minima and maxima varying in which months they occur throughout the record. For example, the peak aerosol occurs in October 2002, August 2003, July 2004 and September 2005. These produce time differences in maximum aerosol of 11, 9 and 14 months respectively. A large spike much greater than the third standard deviation of aerosol occurred in 2008, likely due to the 2008 Northern California wildfires (Gyawali et al. 2009). The 2012 to 2014 drought is highlighted in red and this period shows a very similar and unchanging trend over the three years with peak aerosol occurring in October 2012, September 2013 and October 2014. However, in all every year beginning in 2012, a second maximum occurs during the month of July. This bimodal characteristic of AOD in recent years is likely due to a couple of phenomenon. Since much of the Southern half of California is desert, high winds in the spring and summer cause statewide spikes in AOD (Frank et al. 2007). Another possible producer of peak AOD is the seasonal fire patterns in California. Since California has two dominant wind seasons, the amount of wild fires peak during this time. One peak occurs in October through April and the other occurs from June through September (Jin et al. 2015). Both of these can provide enough airborne aerosol for the state average to reach two maximums throughout the year, however, likely a combination of both dust and fire season is more realistic.

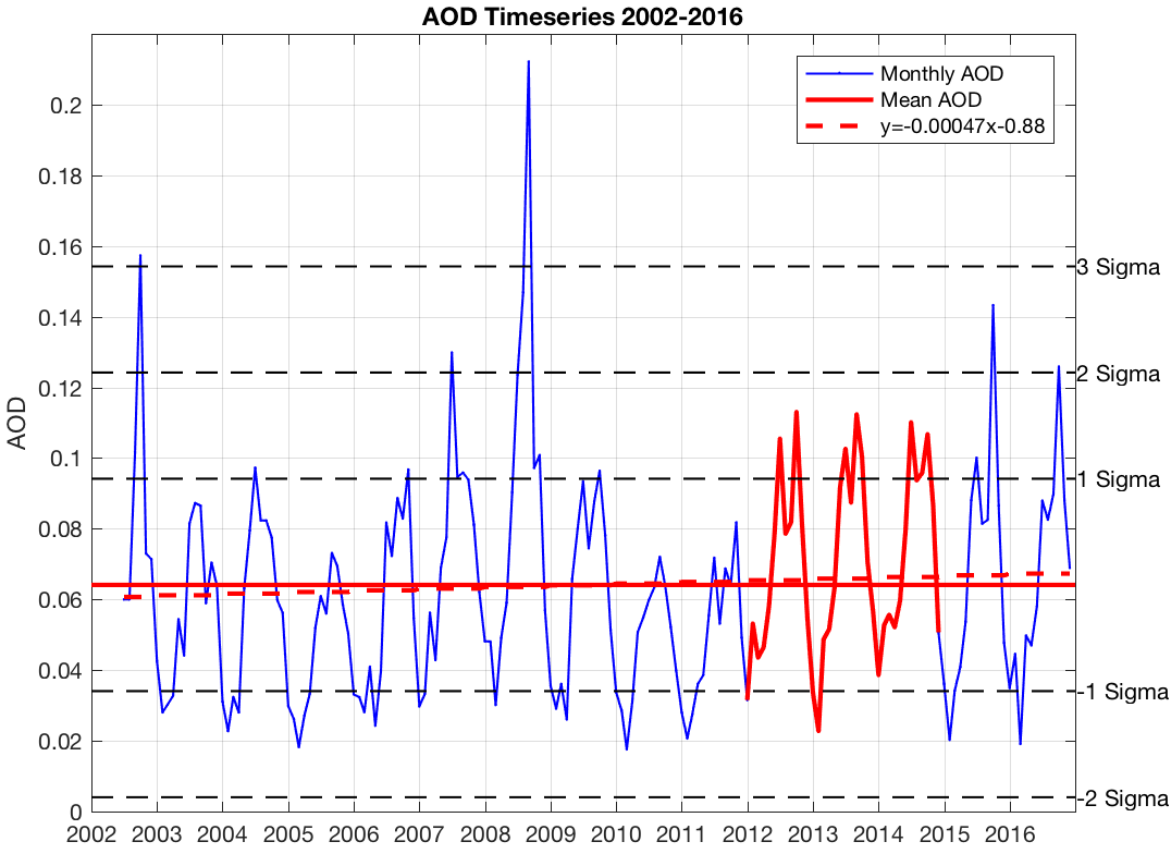

Figure 12. MODIS aerosol time series beginning in 2002 and ending in 2016. The red solid line is the zero line. The black dashed lines demonstrate the first, second and third standard deviations of MODIS AOD. The red region highlights the 2012-2014 drought.

4.4 Northern and Southern California AOD Trends

The 14-year time series of monthly averaged AOD in California showed that all three drought years had similar bimodal peaks, though it is noted that aerosol did not increase during the drought when averaging AOD over the entire state of California. Unfortunately, the NCEI PDSI calculations are averaged over the state making it difficult to distinguish the spatial characteristics of PDSI and aerosol relationships. However, by splitting California into two sections and computing AOD averages for the Northern and Southern halves, the mechanisms that might affect the Northern and Southern halves of California separately can be understood. From Figure 13, the Northern California peak aerosol occurs in August between 2002 and 2016 and Southern California has peaks occurring in May. This addresses the fact that the original AOD double peaks are coming from different parts of the state because separately, the Northern and Southern peaks are in different months. In addition, the different the characteristics of the two halves become apparent. For example, Southern California has a much greater mean (0.0855) AOD than Northern California (0.0432). Also, the 2008 wildfires appear much more prominently in Northern time series than the Southern (Gyawali et al. 2009). This split analysis suggests the need for smaller regions for drought analysis, especially in California where the Northern and Southern halves have many different characteristics.

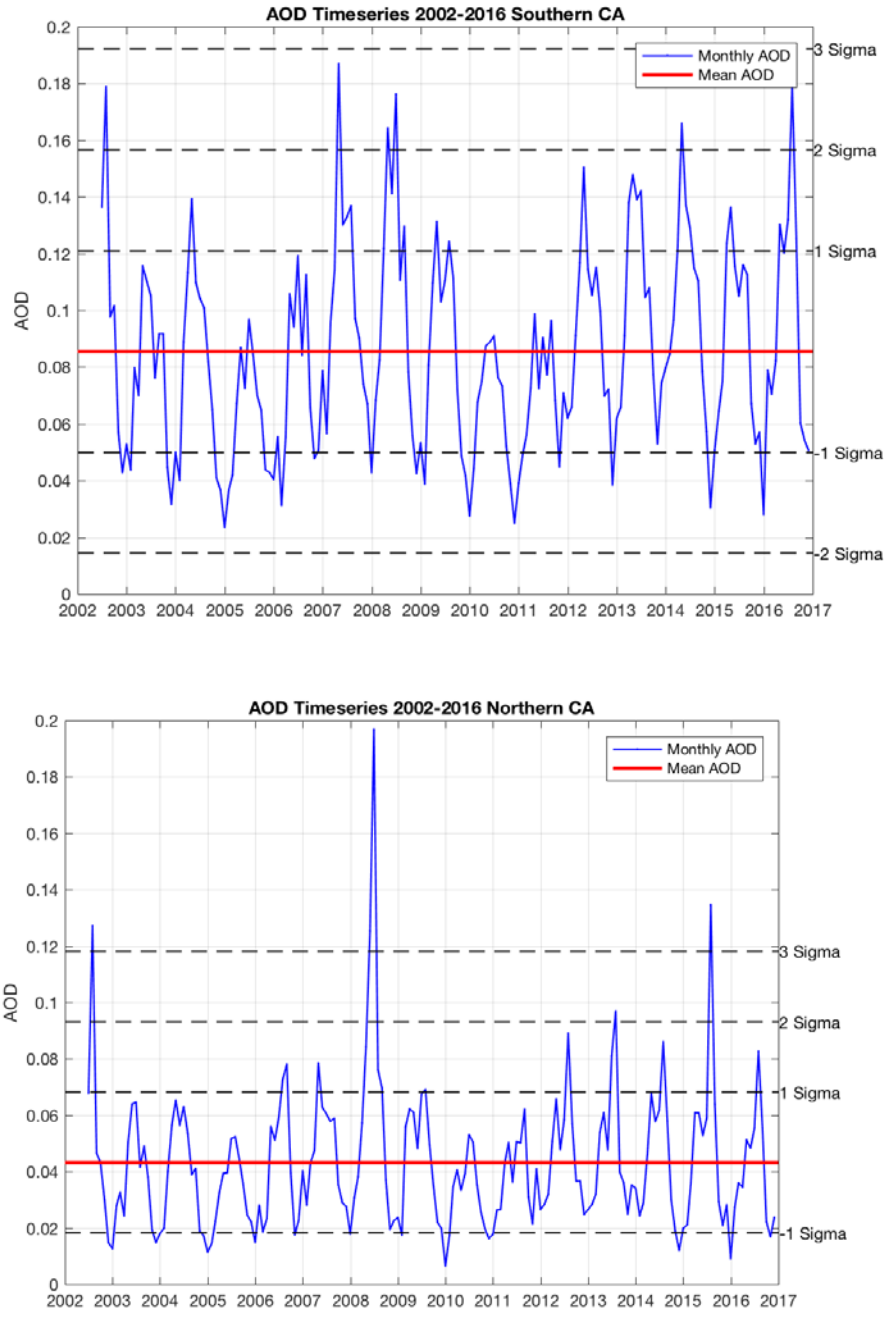

Figure 13. MODIS aerosol time series beginning in 2002 and ending in 2016. The red solid line is the zero line. The black dashed lines demonstrate the first, second and third standard deviations of MODIS AOD. The top panel is averaged over the Northern half of California and the bottom panel is averaged over the Southern half.

4.5 Precipitation Statistical Significance between Five Selected Periods

To address the precipitation differences between drought and non-drought years, the Wilcoxon Mann Whitney Rank Sum-Test was computed for each GPCP and TRMM grid box for the state of California as shown in Figure 13. A period is considered to be significant when compared another period and the z –value is 1, using the Wilcoxon-Mann-Whitney Rank Sum-Test. TRMM data was re-gridded from 0.25 x to 2.5 degree for best comparison to GPCP resolution. Period 1 and 5, because period 1 is a neutral level of PDSI and period 5 is considered to be extreme drought from were selected from Figure 7 for analysis in Figure 13. The results show a similar pattern between the two remote sensing methods, with wetter conditions in the north and drier in the south. Few significant grid boxes with dots to denote significance occur. However, when they occur they tend to be located in the Northern half of California. Table 3 summarizes the percentage of California that shows significant differences in precipitation between the two periods for all combinations of PDSI selection periods. GPCP and TRMM show good agreement from this analysis. However, it is interesting to note that the comparison between periods 3 and 5, both drought periods, have greater than 10% of California as significantly different between the two periods being compared. This is surprising considering all other PDSI selection period comparisons reveal under 10% significant. This result essentially demonstrates the severity of the 2012-2014 drought.

Period 3, a drought, was chosen for many of the comparisons between other PDSI selection periods. However, the results were different than the other drought, period 5. Since these two periods are considered to be in severe drought one would expect that the results show similar precipitation and aerosol patterns. However, period 3 showed much more similarly to period 2 and 4, which are wet periods. Because of the impartial way the PDSI selection

periods were chosen, Period 3 happened to occur during February 2008. Selecting the two months before and after produced an extraction period from December 2007 to April 2008. Through a time-series analysis of precipitation and aerosol not pictured here, greater than normal precipitation occurred during period 3. In addition, there was a drop in aerosol levels, likely caused by precipitation "washing out" aerosol in the atmosphere. A closer look at Figure 7b reveals a small maximum in PDSI between December 2007 and April 2008. This is another example of the greater than normal precipitation occurring during drought yet not increasing to positive PDSI levels.

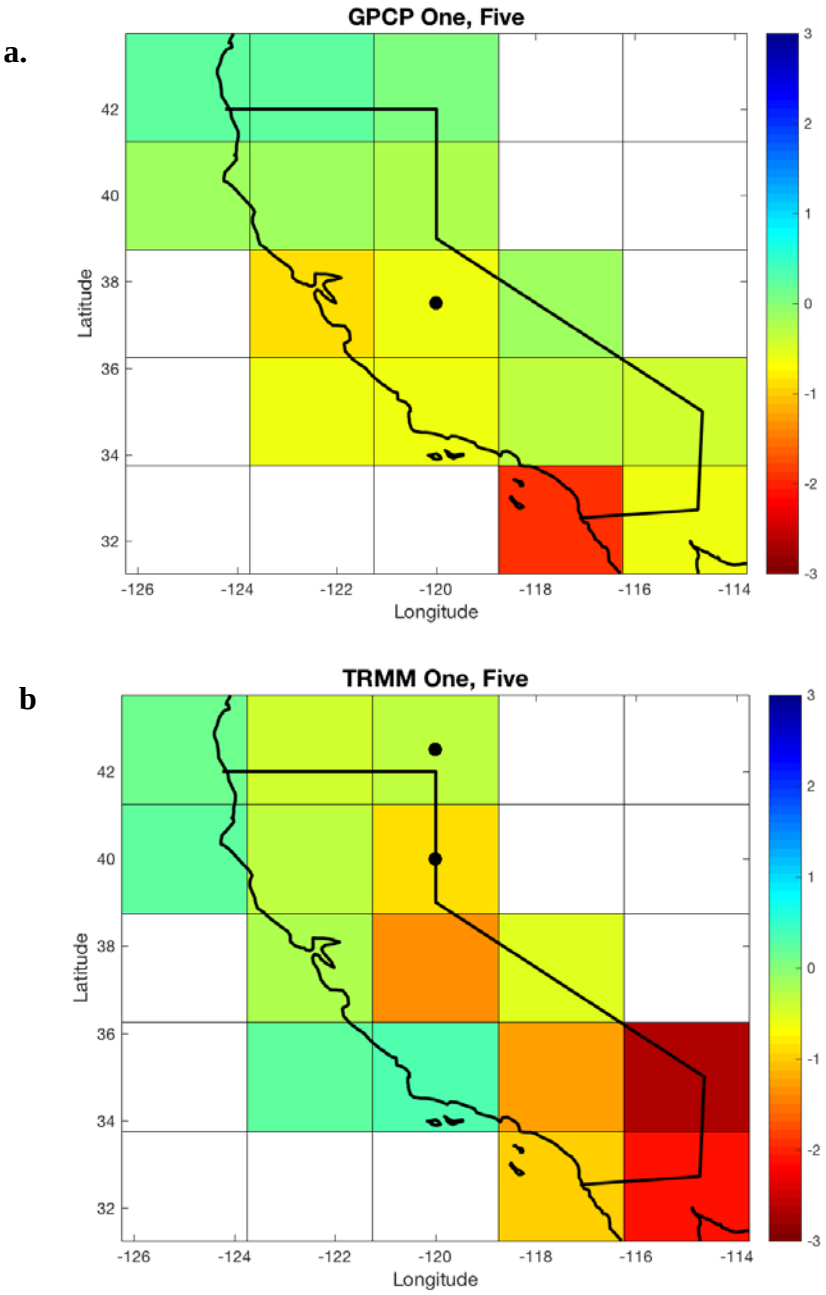

Figure 14. P-values from the computed Wilcoxon Rank-sum test between (a) GPCP Precipitation and (b) TRMM precipitation for periods 1 and 5. The dots show the significantly different regions.

Time Period Number	Category of Time Period	Ratio Significant to total boxes GPCP	Percentage of California GPCP	Ratio Significant to total boxes TRMM	Percentage of California TRMM
1 2	Neutral, Positive PDSI	0/15	0 %	0|15	0 %
1 3	Neutral, Negative PDSI	0/15	0 %	0|15	0 %
1 4	Neutral, Positive PDSI	1/15	6.7 %	0|15	0 %
1 5	Neutral, Negative PDSI	1/15	6.7 %	2|15	6.7 %
2 3	Positive PDSI, Negative PDSI	0/15	0 %	0|15	0 %
2 4	Positive PDSI, Positive PDSI	0/15	0 %	0|15	0 %
2 5	Positive PDSI, Negative PDSI	1/15	6.7 %	0|15	0 %
3 4	Negative PDSI, Positive PDSI	0/15	0 %	0|15	0 %
3 5	Negative PDSI, Negative PDSI	2/15	13.3 %	6|15	40 %
4 5	Positive PDSI, Negative PDSI	7/15	46.7 %	5|15	33.2 %

Table 3. Percentage area (significant boxes to total boxes) of California that shows precipitation significantly different between the two chosen five month periods of time.

4.6 Aerosol Statistical Significance between five selected periods

Each grid box in the MODIS domain was analyzed with a similar method to Section 4.4. Figure 14 shows four examples of comparisons between PDSI selection periods as described in Section 3.3 and Figure 7. By comparing the four PDSI selection periods, we can analyze aerosol during drought and non-drought periods. Period 1, or neutral PDSI, was compared to each of the following wet or dry periods. As the analysis moves through time, it becomes clear that each successive period has significantly different aerosol amounts, whether that means higher during drier periods or lower during wetter periods as compared to the original neutral period.

Furthermore, AOD increases 44 % from 0.0663 to 0.0955 between periods 1 and 5 with the greatest increase in AOD and the highest number of statistically significant gird boxes in Northern California. This suggests that aerosol in Southern California did not change as much as Northern California between periods 1 and 5. As expected, however, there is a large "hot spot" of significantly increased aerosol around Los Angeles, a highly populated and polluted region that is characteristically dry (as seen in Figure 1).

Table 4 summarizes the percent of California that has significantly different distributions of aerosol between the selected time periods. 56 grid boxes of 1 x 1 degree cover the state of California; the percent of significant area is based off this number. This result shows that over time, the number of significant grid boxes increases from 44.6% (period 1) to 69.6% (period 5). In addition, the analysis between periods 4 and 5 reveals that almost all of California has significantly different aerosol.

The Northern Californian region is most significant between all tests of precipitation and aerosol. This is because Northern California was greatly affected by the drought in both aerosol and precipitation. In contrast, Southern California, tends to be drier and has a background state which includes greater concentrations of aerosol. Therefore, the increase in aerosol during

drought years was not as significant as the north. Northern California, however, often sees more rain and less aerosol. The lack of rain is probably the primary reason for the devastation to agricultural productivity. During extreme drought, like the 2012-2014 drought, this aerosol increase is significantly different than both wet and normal years.

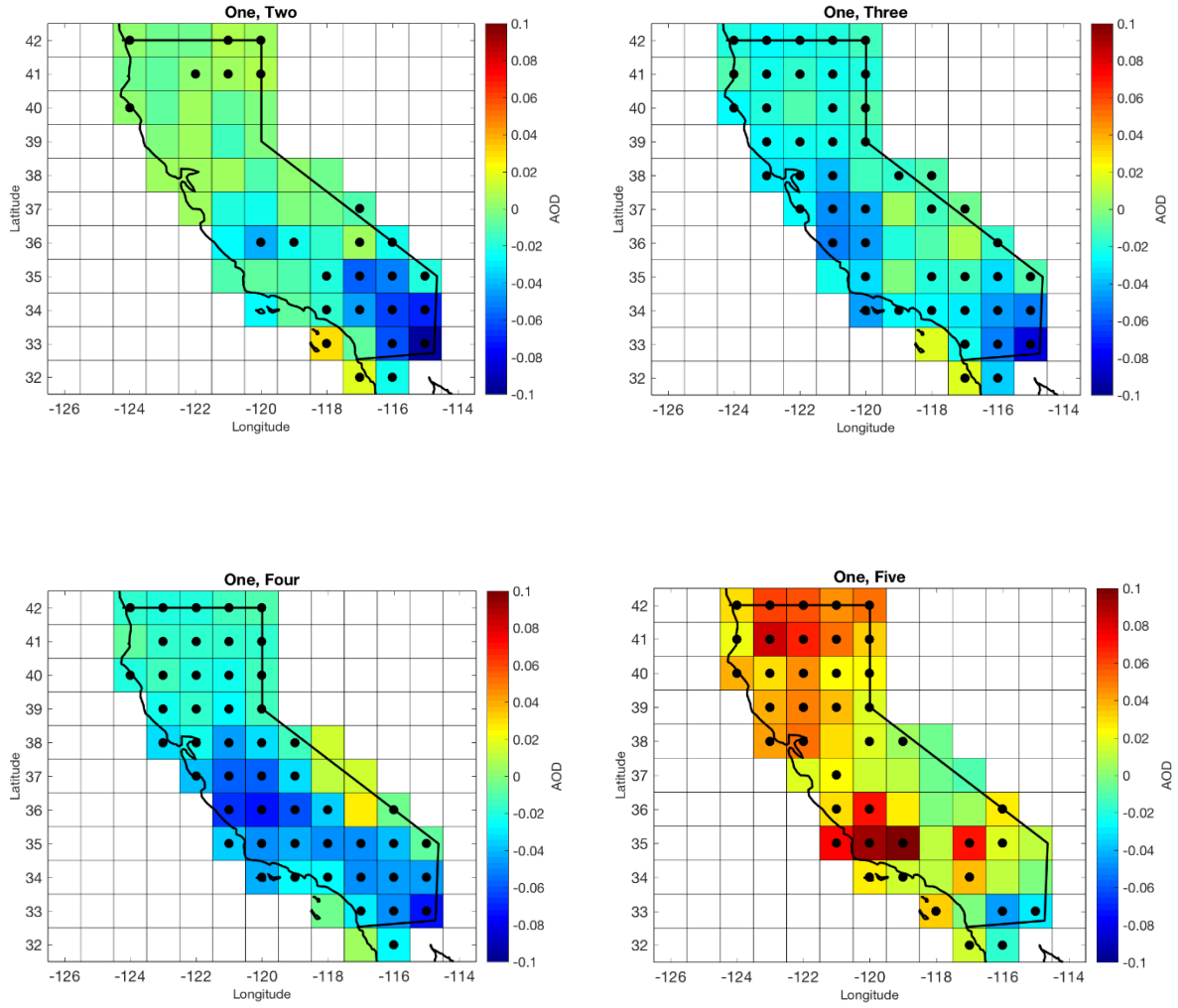

Figure 15. The significant locations (black dots) from the computed Wilcoxon Rank sum test between MODIS AOD during the lowest levels of PDSI for the five months of the drought and MODIS AOD during the highest levels of PDSI for five month periods between 2002 and 2016. The difference between the two time periods is color shaded with greater values in yellow, oranges and red and negative values in green, cyan and blue.

Time Period Number	Category of Time Period	Ratio Significant to total boxes	Percentage of California
1,2	Neutral, Positive PDSI	25/56	44.6%
1,3	Neutral, Negative PDSI	47/56	83.9%
1,4	Neutral, Positive PDSI	49/56	87.5%
1,5	Neutral, Negative PDSI	39/56	69.6%
2,3	Positive PDSI, Negative PDSI	43/56	76.8%
2,4	Positive PDSI, Positive PDSI	50/56	89.2%
2,5	Positive PDSI, Negative PDSI	45/56	80.3%
3,4	Negative PDSI, Positive PDSI	19/56	33.9%
3,5	Negative PDSI, Negative PDSI	53/56	94.6%
4,5	Positive PDSI, Negative PDSI	53/56	94.6%

Table 4. Shows the percentage area (significant boxes to total boxes) of California that shows AOD significantly different between the two chosen 5-month periods of time.

4.7 Sources of Error

A number of sources of error exist including measurement error, spatial sampling error and temporal sampling error. Measurement error is natural in observational studies using remote sensors. However, if this error were to be reduced, remote sensing studies would have greater confidence of the extreme measurements. Spatial resolution was also a potential source of error, higher spatial resolution would have given this study more spatially specific results, this is especially important because of the many differences between Northern and Southern California. Higher temporal sampling would have improved both TRMM and GPCP estimations of precipitation. Satellite-derived averages of precipitation often include significant sampling uncertainties that stem from infrequent satellite overpasses as well as temporal and spatial variability in rain fields.

CHAPTER 5: SUMMARY

5.1 Conclusions

This work quantitatively summarizes the precipitation, drought and aerosol trends in California for 14 years, between 2002 and 2016. Due to the complex nature of drought, data from four sources, including MODIS, TRMM, GPCP and NCEI, were used to investigate the relationship of aerosol and precipitation in drought to non-drought periods. Five-month periods were selected for examination of aerosol and precipitation distributions. From the Wilcoxon Rank-Sum Test, estimates were made as to the percentage of California with significantly different aerosol distributions between the PDSI selected periods. Based on our empirical analysis of satellite and ground based observations, this study found six core results. The following relationships were observed:

- Precipitation rates in California are different in the summer months than in the winter months.
- The 2012-2014 drought was the worst drought in over a century of ground-based observations and well over two standard deviations from the mean PDSI in California.
- The rate of decrease of PDSI between 2002 and 2016 (2.77 PDSI/10 years) is greater than the rate of decrease between 1895 and 2016 (0.121 PDSI/10 years).
- About 70% percent of the state of California shows significantly greater amounts of aerosol between the 2012-2014 drought (period 5) and neutral case in 2002 (period 1).
- Statewide aerosol amount increased between the same periods as above by 44 % This increased aerosol may have caused changes to cloud properties which would

contribute to a situation where clouds would be less likely to produce rain. Precipitation suppression completes a positive feedback loop and a mechanism for which to exacerbate the drought. This conclusion is supported by theoretical relationships found in other studies and Appendix 1 (Albrecht 1989).

- The Northern portion of California is most impacted by aerosol concentrations during drought years. In addition, Northern California showed significant changes in precipitation between drought and non-drought years.

Though it is difficult to fully decouple meteorological influences, this suggests that the mechanisms that produce drought are related to the mechanisms that affect the distribution of aerosol.

Drought in the United States seems to be increasing not only in magnitude but also in complexity (Weiss et al. 2009). Climate projections show a trend towards greater mean temperature and higher extremes, possibly bringing more extreme droughts to California and the world (Gregory et al. 1997). Higher temperatures of even 1-3° C will likely modify the hydrologic budget leading to a change in global precipitation patterns, essentially making dry locations drier and wet areas wetter (IPCC 2014). These trends are driven by anthropogenic emissions of greenhouse gases due to growing populations which are increasing demand on fossil fuels. It is clear that drought will play an increasingly important role in the future.

5.2 Future Work

The results from this study validate the need for further investigation of drought, particularly in the context of aerosol-cloud interactions. Although large scale satellite surveys provide invaluable temporal and spatial microphysical information, measurement errors still exist. Future work in this area will focus on factors contributing to increased aerosol during drought periods.

Future topics of interest include:

- Scientific studies about the relationship between drought and the El Niño Southern Oscillation (ENSO). The 2012-2014 drought overlapped with one of worst El Niño periods on record (Wang et al. 2014). Understanding large scale climate fluctuations may help provide answers about the changes in temperature and precipitation that affect drought.
- A longer aerosol record is necessary for results with higher confidence. Unfortunately, aerosol measurements from remote sensors do not provide enough data for long-term climatological studies. Future droughts will lead to more opportunities for similar analysis.
- Synoptic level analysis of weather patterns during drought may give insight into aerosol sources. A key weather aspect to initiate drought is blocking ridges in the upper atmosphere.
- There is a need for improvement in the measurement of aerosol from remote sensors. Vertical distributions of aerosol with high spatial, global coverage and temporal resolution could provide additional information about cloud and aerosol relationships.
- A more comprehensive version of PDSI is necessary. Drought is a regional phenomenon that is highly dependent on land surface characteristics. Perhaps a drought index designed especially for the regional atmospheric and land characteristics of California is necessary.

Considering drought events tend to occur in California every 3-5 years, the frequency of this phenomenon warrants greater effort in drought mitigation.

This work provides only the framework for future studies. It provides a strong base for understanding the changes in aerosol amount during drought and why those changes occur. Future studies, observations and models are necessary for the building of a comprehensive understanding of drought in California.

APPENDIX 1

Since aerosols modify cloud properties, with ramifications for the formation of precipitation, it is necessary to evaluate how aerosol impacts the microphysical structure of clouds. A key microphysical characteristic of clouds that is modified by aerosol amount is cloud droplet size. Satellite observations can provide a detailed view of aerosol, cloud and precipitation relationships. A commonly used space borne estimate of cloud drop size is cloud drop effective radius (CER). CER is the weighted mean of the size distribution of cloud drops and represents the mean cloud particle size. Various satellite-based remote-sensing techniques exist for monitoring global CER from space. A case study was completed to understand the relationship between CER and AOD in California during the 2014 drought year and a corresponding wet period occurring in 2010. We investigate aerosol-cloud impacts during drought and non-drought periods in California in three regional subsets: the entire state (Test 1), the Northern portion (Test 2), and the Southern portion (Test 3).

This analysis will use MODIS data, as described in Chapter 2.2. Specifically, for this analysis we will be using MODIS AOD, and MODIS Level 3 Version C6 CER with product name Aerosol_Optical_Depth_Land_Ocean_Mean and Cloud_Effective_Radius_Liquid_Mean were obtained from https://ladsweb.modaps.eosdis.nasa.gov/ (Platnick et al. 2003). MODIS CER is provided at 1 x 1 degree resolution and is derived using the MODIS visible, near-infrared, and shortwave infrared bands including the water absorbing bands at 1.6, 2.1 and 3.7 μm and one non-absorbing band of 0.65 μm (Platnick et al. 2003).

Possible errors in our interpretation of aerosol-cloud interactions occur because of the fact that MODIS aerosol cannot be detected when clouds are present. Basically, it is impossible to measure both aerosol and cloud properties from MODIS at the same time. The clouds will act

to block any signal from below the cloud layer. However, this problem may be mitigated by the fact that aerosol amount is relatively homogenous when compared to cloud spatial distribution (Yuan et al. 2008). This means that some aerosol quantities within a grid box may be representative of the entire grid box without occurring great error.

Two periods were chosen from the PDSI values for California: one dry period with negative PDSI and one wet period with positive PDSI. From Figure 7, the driest period of the 2012-2014 drought occurred in the summer months of 2014 therefore June, July and August (JJA) chosen to represent a characteristic drought period. Working backwards, the last period with maximum positive PDSI occurred in the winter months of 2010 so December, January and February (DJF) were chosen to represent a "wet" period. By comparing these two 3-month seasons, we can interpret the relationship between aerosol and clouds, and as well as PDSI and aerosol in drought and wet periods.

The study region is the state of California and it is characterized by numerous vegetative and land cover types. Northern California consists of mixed forested regions, while Southern California is mostly desert and grasslands as seen in Figure 1. Because California exhibits both large anthropogenic and natural sources, spatial precipitation and AOD distributions are variable throughout the state. To address this issue, the data was sub-setted to reflect the differences in the Northern and Southern portions of the state. For each day, an area roughly 12.5 x 12.5 degrees was extracted encompassing California. Then, an ocean and land mask was created to fit the extracted data and applied. This masks hides parts of Nevada, Arizona, Oregon, Mexico and the Pacific Ocean. An example of this mask is shown in Figure A1. The daily MODIS data was spatially averaged for three regions which included the entire state (Test 1), the northern half

(Test 2) and the Southern half (Test 3). This sub-setting of the data in these three scenarios will allow for spatial analysis of the relationship of AOD and CER in California.

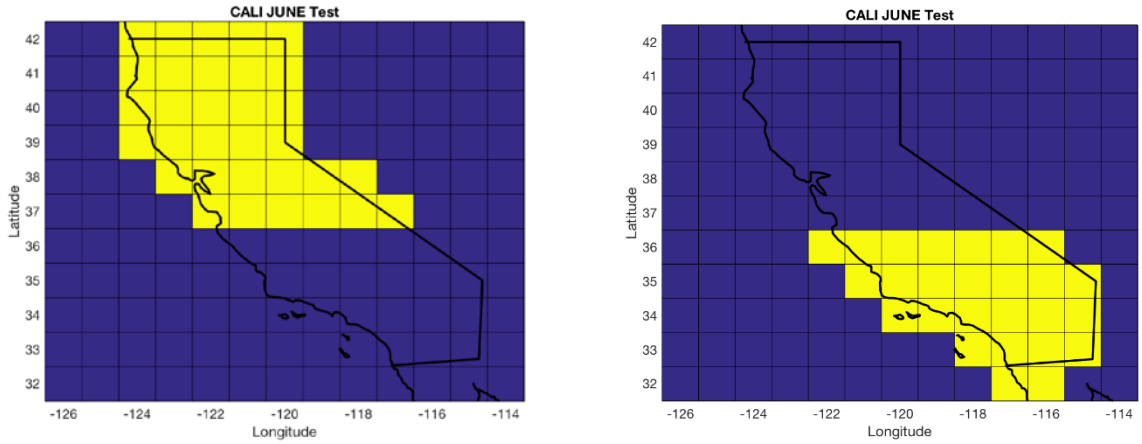

Figure A1. Images showing the grid boxes that encompass the Northern and Southern regions of California. Green represents the area that was spatially averaged for Test 2 and Test 3.

Histograms of AOD and CER for the three tests are shown in Figure A2, A3 and A4. Figure A2 examines the relationships between AOD and CER for the entire state of California (Test 1). The CER histogram spread is between 6 and 22 µm. Peak or the most common values, occur between 11 and 13 µm for JJA 2014 and between 15 and 17 µm for DJF 2010. It is clear that the JJA 2014 CER values are shifted to smaller CER then the DJF 2010 values. Peak AOD occurs between 0.05 and 0.15 and varies between 0 and 0.6. In addition, there is a slight increase of 0.01 of AOD between DJF 2010 and JJA 2014. JJA 2014 has AOD values greater than 0.3. DJF 2010 shows no AOD observations greater than 0.3.

Figure A3 shows the same analysis for the northern region of California. The most frequently occurring CER size for DJF occurs at 36 µm while the JJA CER peaks at 27 µm. In other words, the distribution is shifted to smaller size cloud drops by about 9 µm between DJF

2010 and JJA 2014. In both cases, CER varies between 7 and 23 µm. Test 2 shows the same pattern as Test 1 occurs with peak JJA 2014 AOD values are shifted to slightly higher levels than peak DJF 2010 AOD values by about 0.1. Large maximum AOD values are present in JJA 2014 when compared to the DJF 2014 varying between 0.3 and 0.6.

Test 3, for the Southern California region, is shown in Figure A4. The DJF 2010 Southern California CER values have peak at 29 µm while the JJA 2014 analysis peaks at 25 µm. However, JJA 2014 is shifted to smaller CER by about 5 µm. The width of the JJA 2014 distribution is between 7 and 19 µm but the DJF 2010 distribution width is between 7 and 23 µm. Test 3 has similar results to Figure A3 with JJA 2014 shows a much larger maximum AOD value than its corresponding wet period of DJF 2010, however, not to the extent of Test 2. Similar to Test 2, the peak AOD values in JJA 2014 and DJF 2010 occur between 0.1 and 0.15 and 0.05 and 0.1 respectively.

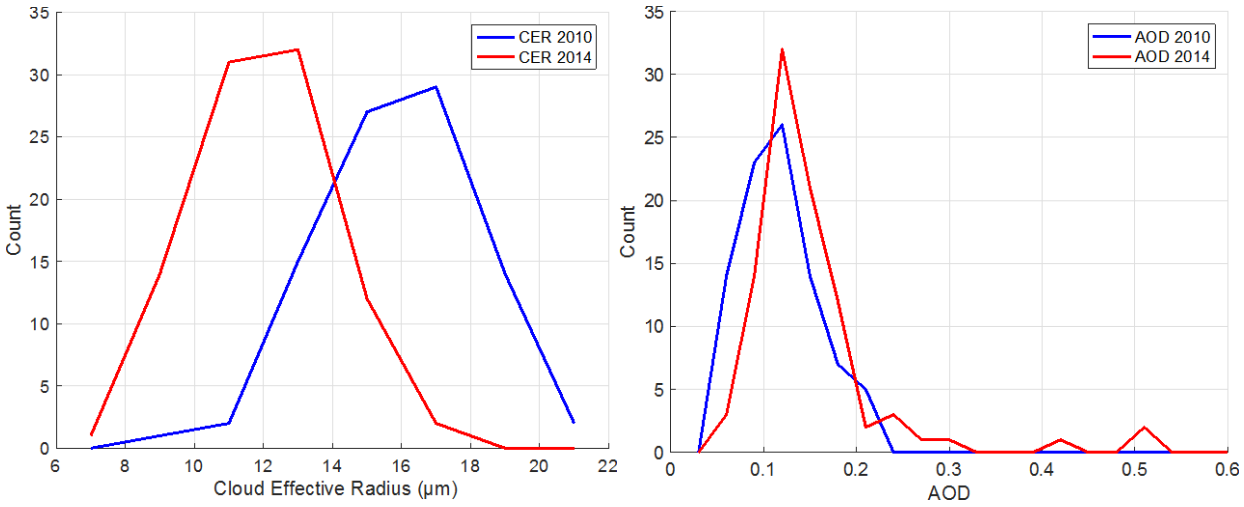

Figure A2. Histograms of AOD and CER for DJF 2010 and JJA 2014 averaged for the entire state of California.

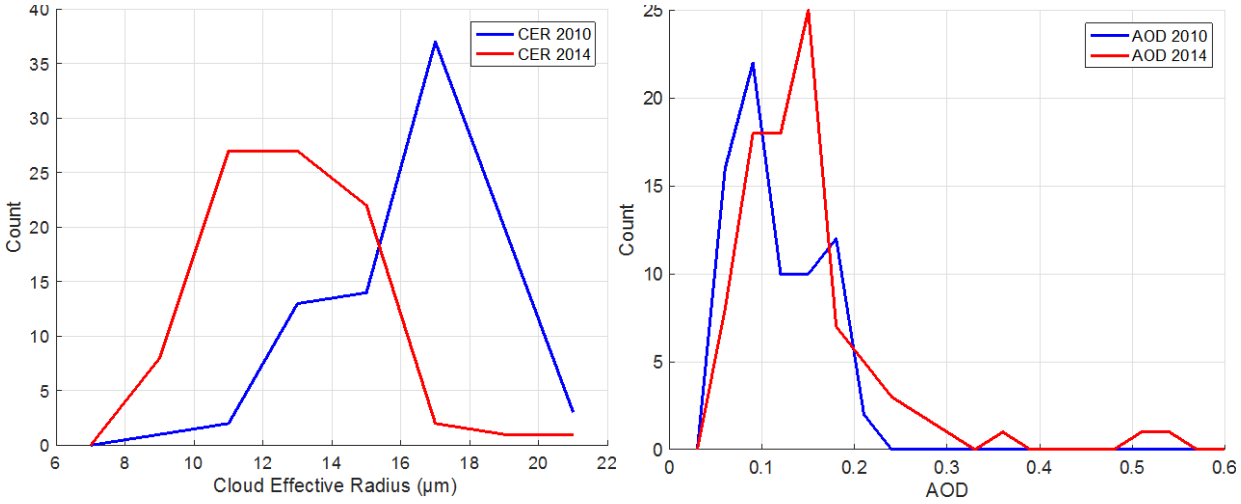

Figure A3. Histograms of AOD and CER for DJF 2010 and JJA 2014 averaged for the Northern half California.

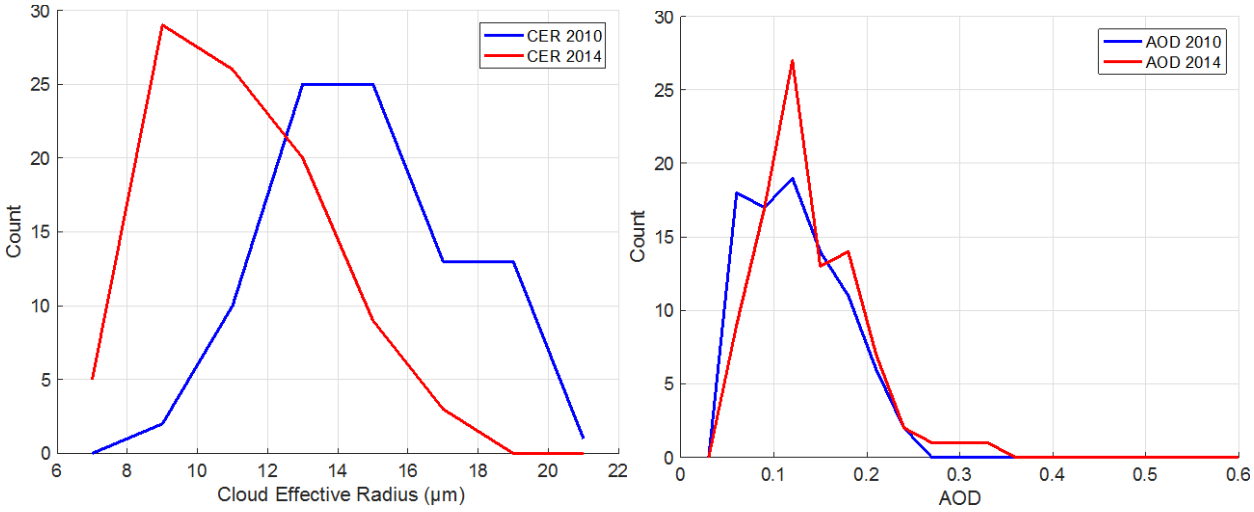

Figure A4. Histograms of AOD and CER for DJF 2010 and JJA 2014 averaged for the Southern half California.

This case study examined the effects of aerosol loading and cloud properties a wet and a dry season in California. Using MODIS L3 daily AOD and CER data two time periods were selected as representative drought (JJA 2014) and non-drought years (DJF 2010). Three different tests of these periods were completed to represent different study regions (state-wide, Northern and Southern). Our examination of the dependence of CER on AOD allows for the rough calculation of the indirect effects aerosols have on the atmosphere.

In 1977, Twomey hypothesized that cloud particle size is reduced by adding aerosols as cloud condensation nuclei (CCN) for a fixed liquid water amount (Twomey 1977). This theory is confirmed in all tests. The CER was smaller during the JJA 2014 drought period than the DJF 2010 period with aerosol showing a slight increase. This finding is in fact consistent with Twomey's theory and suggests precipitation suppression is possible during dry conditions when greater aerosol is present (Twomey 1974). Test 3 demonstrated that Southern California sees smaller cloud effective radius in both drought and non-drought periods. In addition, the results show that the greatest levels of aerosol were seen in the Northern portion of the state during the summer months of 2014. Figure 8 shows that Northern California is normally wetter than Southern California. The fact that maximum aerosol is present during the drought is concerning. This suggests that Northern California is abnormally dry and that the chance for the aerosol to loft and become airborne is easier than it is during non-drought periods. These findings prove a negative dependence of cloud particles size on aerosol loading during drought periods when compared to non-drought periods.

CHAPTER 6: REFERENCES

Adler, R. F., G. J. Huffman, D. Bolvin, E. Nelkin, and S. Curtis, 1999: Comparison of TRMM and Global Precipitation Climatology Project (GPCP) Precipitation Analyses. *NASA Tech. Reports*, 7–8.

——, and Coauthors, 2003: The Version-2 Global Precipitation Climatology Project (GPCP) Monthly Precipitation Analysis (1979–Present). *J. Hydrometeorol.*, **4**, 1147–1167, doi:10.1175/1525-7541(2003)004<1147:TVGPCP>2.0.CO;2. http://journals.ametsoc.org/doi/abs/10.1175/1525-7541%282003%29004%3C1147%3ATVGPCP%3E2.0.CO%3B2.

Albrecht, B. A., 1989: Aerosols, Cloud Microphyics and Fractional Cloudiness. *Science.*, **245**, 1227–1230. https://doi.org/10.1126/science.245.4923.1227.

Alley, W. M., 1984: The Palmer Drought Severity Index: Limitations and Assumptions. *J. Clim. Appl. Meteorol.*, **23**, 1100–1109.

Ault, A. P., C. R. Williams, A. B. White, P. J. Neiman, J. M. Creamean, C. J. Gaston, F. M. Ralph, and K. A. Prather, 2011: Detection of Asian dust in California orographic precipitation. *J. Geophys. Res. Atmos.*, **116**, 1–15, doi:10.1029/2010JD015351.

Cayan, D., and J. Roads, 1984: Local Relationships between United States West Coast Precipitation and Monthly Mean Circulation Parameters. *Mon. Weather Rev.*, **112**, 1276–1282, doi:10.1175/1520-0493(1984)112<1276:LRBUSW>2.0.CO;2.

Chu, P. S., and H. Chen, 2005: Interannual and interdecadal rainfall variations in the Hawaiian Islands. *J. Clim.*, **18**, 4796–4813, doi:10.1175/JCLI3578.1.

Diffenbaugh, N. S., D. L. Swain, and D. Touma, 2015: Anthropogenic warming has increased drought risk in California. *Proc. Natl. Acad. Sci.*, **112**, 3931–3936, doi:10.1073/pnas.1422385112.

Frank, T. D., L. Di Girolamo, and S. Geegan, 2007: The spatial and temporal variability of aerosol optical depths in the Mojave Desert of southern California. *Remote Sens. Environ.*, **107**, 54–64, doi:10.1016/j.rse.2006.06.024.

Gregory, J. M., J. F. B. Mitchell, and A. J. Brady, 1997: Summer drought in Northern Midlatitudes in a time-dependent CO2 climate experiment. *J. Clim.*, **10**, 662–686, doi:10.1175/1520-0442(1997)010<0662:SDINMI>2.0.CO;2.

Griffin, D., and K. J. Anchukaitis, 2014: How unusual is the 2012 – 2014 California drought? *AGU Geophys. Res. Lett.*, **41**, 9017–9023, doi:10.1002/2014GL062433.1.

Guttman, N., and R. Quayle, 1995: A Historical Persepective of U.S. Climate Divisions. *Bull. Am. Meteorol. Soc.*, **77**, 293–202.

Gyawali, M., W. P. Arnott, K. Lewis, and H. Moosmüller, 2009: In situ aerosol optics in Reno, NV, USA during and after the summer 2008 California wildfires and the influence of aerosol coatings. *Atmos. Chem. Phys. Discuss.*, **9**, 8007–8015, doi:10.5194/acp-9-8007-2009.

Howitt, R., J. Medellín-azuara, D. Macewan, and D. A. Lund, J.R. and Sumner, 2014: Economic Analysis of the 2014 Drought for California Agriculture. http://watershed.ucdavis.edu.

Hsu, N. C., M. Jeong, C. Bettenhausen, A. M. Sayer, R. Hansell, C. S. Seftor, J. Huang, and S. Tsay, 2015: Enhanced Deep Blue aerosol retrieval algorithm : The second generation. *J. Geophys. Res. Atmos.*, **118**, 9296–9315, doi:10.1002/jgrd.50712.

Huffman, G. J., and D. T. Bolvin, 2017: *Real-Time TRMM Multi-Satellite Precipitation Analysis Data Set Documentation*. Mesoscale Atmospheric Processes Laboratory, 1-48 pp.

Huffman, G. J., and Coauthors, 1997: The Global Precipitation Climatology Project (GPCP) Combined Precipitation Dataset. *Bull. Am. Meteorol. Soc.*, **75**, 5–20, doi:10.1175/1520-0477(1997)078<0005:TGPCPG>2.0.CO;2.

IPCC, 2014: Intergovernmental Panel on Climate Change (IPCC): Clouds and Aerosols. *Contrib. Work. Groups I, II III to Fifth Assess. Rep. Intergov. Panel Clim. Chang.*, **5**.

Jin, Y., M. Goulden, S. Faivre, V. Veraverbeke, A. Hall, M. Hand, S. Hook, and J. Randerson, 2015: Identification of two distinct fire regimes in southern California: implications for economic impact and future change. *Environ. Res. Lett.*, **10**, doi:10.1088/1748-9326/10/9/094005.

Karl, T., F. Quinlan, and D. S. Ezell, 1987: Drought Termination and Amelioration: It's Climatological Probability. *J. Clim. Appl. Meteorol.*, **26**, 1198–1209, doi:10.1175/1520-0450(1987)026<1198:DTAAIC>2.0.CO;2.

Kaufman, Y. J., D. Tanre, M. Herman, and S. Mattoo, 1997: Remote sensing of aerosol properties over oceans using the MODIS / EOS spectral radiances. *J. Geophys. Res. Atmos.*, **102**, 16971–16988, doi:10.1029/96JD03437.

Koren, I., Y. J. Kaufman, D. Rosenfeld, and L. A. Remer, 2005: Aerosol invigoration and restructuring of Atlantic convective clouds. *Geophys. Res. Lett.*, **32**, 4–7, doi:10.1029/2005GL023187.

Koren, I., G. Feingold, and L. A. Remer, 2010: The invigoration of deep convective clouds over the Atlantic : aerosol effect, meteorology or retrieval artifact. *Atmos. Chem. Phys.*, **10**, 8855–8872, doi:10.5194/acp-10-8855-2010.

Kummerow, C., and W. Barnes, 1998: The Tropical Rainfall Measuring Mission (TRMM) Sensor Package. *J. Atmos. Ocean. Technol.*, **15**, 809–817.

Levy, R. C., R. Kahn, R. C. Levy, G. G. Leptoukh, R. Kahn, V. Zubko, A. Gopalan, and L. A. Remer, 2009: A Critical Look at Deriving Monthly Aerosol A Critical Look at Deriving Monthly Aerosol Optical Depth From Satellite Data. *IEEE Trans. Geosci. Remote Sens.*, **47**, 2942–2956, doi:10.1109/TGRS.2009.2013842.

Levy, R. C., L. A. Remer, R. G. Kleidman, S. Mattoo, C. Ichoku, R. Kahn, and T. F. Eck, 2010: Global evaluation of the Collection 5 MODIS dark-target aerosol products over land. *Atmos. Chem. Phys.*, **10**, 10399–10420, doi:10.5194/acp-10-10399-2010.

Li, Z., F. Niu, J. Fan, Y. Liu, D. Rosenfield, and Y. Ding, 2011: Long-term impacts of aerosol on the vertical development of clouds and precipitation. *Nat. Geosci.*, **4**, 888–894.

Lohmann, U., 2006: Aerosol effects on clouds and climate. *Space Sci. Rev.*, **125**, 129–137, doi:10.1007/s11214-006-9051-8.

Lowenthal, D. H., R. D. Borys, W. Cotton, S. Saleeby, S. A. Cohn, and W. O. J. Brown, 2011: The altitude of snow growth by riming and vapor deposition in mixed-phase orographic clouds. *Atmos. Environ.*, **45**, 519–522, doi:10.1016/j.atmosenv.2010.09.061. http://dx.doi.org/10.1016/j.atmosenv.2010.09.061.

Lynn, B., A. Khain, D. Rosenfeld, and W. L. Woodley, 2007: Effects of aerosols on precipitation from orographic clouds. *J. Geophys. Res. Atmos.*, **112**, n. page, doi:10.1029/2006JD007537.

Mann, H. B., and W. D. R., 1947: Institute of Mathematical Statistics is collaborating with JSTOR to digitize, preserve, and extend access to The Annals of Mathematical Statistics. *Statistics (Ber).*, **18**, 50–60.

NCEI, 2011: Climate at a Glance: U.S. Time Series. *NOAA Natl. Centers Environ. Inf.*, Monthly Temperatures, Precipitation, PDSI for Cali.

Neiman, P. J., F. M. Ralph, G. A. Wick, J. D. Lundquist, and M. D. Dettinger, 2008:

Meteorological Characteristics and Overland Precipitation Impacts of Atmospheric Rivers Affecting the West Coast of North America Based on Eight Years of SSM/I Satellite Observations. *J. Hydrometeorol.*, **9**, 22–47, doi:10.1175/2007JHM855.1. http://journals.ametsoc.org/doi/abs/10.1175/2007JHM855.1.

Nesbitt, S. W., and A. M. Anders, 2009: Very high resolution precipitation climatologies from the Tropical Rainfall Measuring Mission precipitation radar. *Geophys. Res. Lett.*, **36**, 1–5, doi:10.1029/2009GL038026.

Palmer, W., 1965: Meteorological Drought. **45**, n. page.

Platnick, S., M. D. King, S. A. Ackerman, W. P. Menzel, B. A. Baum, J. C. Riédi, and R. A. Frey, 2003: The MODIS cloud products: Algorithms and examples from terra. *IEEE Trans. Geosci. Remote Sens.*, **41**, 459–472, doi:10.1109/TGRS.2002.808301.

Radke, L. F., P. V. Hobbs, M. W. Eltgroth, L. F. Radke, P. V. Hobbs, and M. W. Eltgroth, 1980: Scavenging of Aerosol Particles by Precipitation. *J. Appl. Meteorol.*, **19**, 715–722, doi:10.1175/1520-0450(1980)019<0715:SOAPBP>2.0.CO;2. http://journals.ametsoc.org/doi/abs/10.1175/1520-0450%281980%29019%3C0715%3ASOAPBP%3E2.0.CO%3B2.

Ramanathan, V., P. J. Crutzen, J. T. Kiehl, and D. Rosenfeld, 2013: Aerosols , Climate , and the Hydrological Cycle. *Science* ., **294**, 2119–2124.

Remer, L. ., and Coauthors, 2005: The MODIS Aerosol Algorithm, Products, and Validation. *J. Atmos. Sci. Sel.*, **62**, 947–973, doi:10.1175/JAS3385.1.

Remer, L. A., and Y. J. Kaufman, 2006: Physics Aerosol direct radiative effect at the top of the atmosphere over cloud free ocean derived from four years of MODIS data. *Atmos. Chem. Phys.*, **6**, 237–253, doi:10.5194.

Remer, L. A., and Coauthors, 2008: Global aerosol climatology from the MODIS satellite sensors. *J. Geophys. Res. Atmos.*, **113**, 1–18, doi:10.1029/2007JD009661.

Rosenfeld, D., and Coauthors, 2008: Flood or Drought : How Do Aerosols Affect Precipitation. *Science.*, **5**, 1309–1313, doi:10.1126/science.1160606.

Sorooshian, A., G. Feingold, M. D. Lebsock, H. Jiang, and G. L. Stephens, 2009: On the precipitation susceptibility of clouds to aerosol perturbations. *J. Geophys. Res.*, **36**, 1–5, doi:10.1029/2009GL038993.

Svoboda, M., M. J. Hayes, D. A. Wilhite, M. D. Svoboda, and M. J. Hayes, 2007: Understanding the Complex Impacts of Drought : A Key to Enhancing Drought Mitigation and preparedness. *Water Resour. Manag.*, **21**, 763–774, doi:10.1007/s11269-006-9076-5.

Thornthwaite, C. W., 1948: An Approach toward a Rational Classification of Climate. *Geogr. Rev.*, **38**, 55–94.

Twomey, S., 1974: Pollution and the Planetary Albedo. *Atmos. Environ.*, **8**, 1251–1256.

——, 1977: The Influence of Pollution on the Shortwave Albedo of Clouds. *J. Atmos. Sci.*, **34**, 1149–1152, doi:10.1175/1520-0469(1977)034<1149:TIOPOT>2.0.CO;2. http://journals.ametsoc.org/doi/abs/10.1175/1520-0469%281977%29034%3C1149%3ATIOPOT%3E2.0.CO%3B2.

U.S. Census, 2016: American Community Survey 1-year estimates. *Census Report. Profile page Calif.*, n. page. https://censusreporter.org/profiles/04000US06-california/.

Wang, S. Y., L. Hipps, R. R. Gillies, and J. H. Yoon, 2014: Probable causes of the abnormal ridge accompanying the 2013-2014 California drought: ENSO precursor and anthropogenic warming footprint. *Geophys. Res. Lett.*, **41**, 3220–3226, doi:10.1002/2014GL059748.

Weiss, J. L., C. L. Castro, and J. T. Overpeck, 2009: Distinguishing pronounced droughts in the

southwestern united states: Seasonality and effects of warmer temperatures. *J. Clim.*, **22**, 5918–5932, doi:10.1175/2009JCLI2905.1.

Westerling, A. L., and T. W. Swetnam, 2003: Interannual to decadal drought and wildfire in the western United States. *Eos, Trans. Am. Geophys. Union*, **84**, 545, doi:10.1029/2003EO490001.

Wilcoxon, F., 1945: Individual Comparisons by Ranking Methods. *Biometrics Bull.*, **1**, 80, doi:10.2307/3001968. http://www.jstor.org/stable/10.2307/3001968?origin=crossref.

Wilhite, D. A., M. V. K. Sivakumar, and R. Pulwarty, 2014: Managing drought risk in a changing climate: The role of national drought policy. *Weather Clim. Extrem.*, **3**, 4–13, doi:10.1016/j.wace.2014.01.002. http://dx.doi.org/10.1016/j.wace.2014.01.002.

Yuan, T., Z. Li, R. Zhang, and J. Fan, 2008: Increase of cloud droplet size with aerosol optical depth: An observation and modeling study. *J. Geophys. Res.*, **113**, D04201, doi:10.1029/2007JD008632. http://doi.wiley.com/10.1029/2007JD008632.